Development of Microfluidic Pipette Tips for Automated Electroporation

By

Rameech Nashana McCormack

B.S. Mechanical Engineering
B.S. Aerospace Engineering
University of Central Florida, 2015

Submitted to the Department of Mechanical Engineering in Partial Fulfillment of the Requirements for the Degree

of

Masters of Science in Mechanical Engineering

at the

Massachusetts Institute of Technology

June 2018

Signature redacted

Signature of Author..... .....
Rameech McCormack
Department of Mechanical Engineering
May 25, 2018

Signature redacted

Certified by..... .....
Cullen Buie
Associate Professor of Mechanical Engineering
Thesis Supervisor

Signature redacted

Accepted by..... .....
Rohan Abeyaratne
Professor of Mechanical Engineering
Quentin Berg Professor of Mechanics; Graduate Officer

Development of Microfluidic Pipette Tips for Automated Electroporation

by

Rameech Nashana McCormack

Submitted to the Department of Mechanical Engineering

On May 25, 2018, in partial fulfillment of the

requirements for the degree of

Master of Science in Mechanical Engineering

Abstract

Genetic engineering and synthetic biology are often used to create microorganism that can produce novel pharmaceuticals, biofuels, and other high value compounds. One of the biggest challenges to advancing the field is the difficulty at which exogenous material is transferred to the cells. Flow-through microfluidic technology has been shown to improve the transformation efficiency and the potential to increase the rate of cell transfection approximately 10,000X the current state of the art. The next step in engineering the process is to scale the microfluidic technology to one that can be incorporated into a high volume genetic engineering environment similar to those used in industry. In this thesis, the development of a high throughput, scalable design is undertaken. Various iterations of the design scheme are taken into account, such as a continuous-flow design for high volume genetic engineering and a microfluidic pipette that interfaces with preexisting liquid handling systems. The design efficacy is also confirmed with experimental tests. The microfluidic pipette tips out-perform the current state of the art (cuvettes) technology. The maximum output transformation efficiency of *Escherichia coli* DH10β, for the fabricated microfluidic pipette tips, is 6.4×10^9 colony forming units per micro-gram of DNA ($CFU/\mu g_{DNA}$).The maximum output performance of the cuvette electroporation process was 2.5×10^9 $CFU/(\mu g_{DNA})$. The performance of the microfluidic tips is 2.5X the output efficiency of the cuvettes at the same applied potential difference and DNA concentration. Further experiments studied the effects of polarity and applied waveform on the transformation efficiency of *Escherichia coli* DH10β. Results of this work indicate that a unipolar waveform and negative polarities increase the transformation efficiency.

Thesis Supervisor: Dr. Cullen R. Buie

Title: Assistant Professor

Acknowledgements

I would like express the greatest gratitude towards my advisor, Professor Cullen Buie, for practicing the highest degree of patience and encouragement. Also, thanks to the entire LEMI research group for their support in all aspects. Thanks to Dr. Paulo A. Garcia and Mahnoor Mirza for their support and collaborative mindset throughout the completion of this work. My sincere appreciation will also be expressed to Leslie Regan for her undying will to help me to succeed.

I will take this time to show my appreciation for my kin and future kin. Your presence and future presence are what motivates me. May you strive to do better, be better, challenge all those that will define you. I hope you will never subscribe to opinions of others. I hope you take steps much bolder than mine and redefine your name.... our name! To Herma, Castel, Shaka, Ricardo, Andre, Demarri, and many, many more!

Thanks to MIT for what I would consider... a valuable experience.

Contents

List of Figures

List of Tables

Chapter 1

Introduction

1.1: Genetic Engineering Overview

Transformation is the process by which exogenous material is introduced into prokaryotic cells. Transformation of bacteria by use of foreign molecules, compounds, deoxyribonucleic acid (DNA) and or proteins into prokaryotic cells is accomplished through various mechanisms. Transformation can occur through naturally occurring phenomena such as transduction and conjugation. Transduction is the transformation of bacteria by means viruses or viral vectors, where the virus have specialized mechanism to transfer genetic material through the cytoplasmic membrane. Conjugation is the transformation of bacteria by means of cell-to-cell contact between a donor cell and a recipient cell. In addition to these two method of horizontal gene transfer, electroporation is a genetic engineering technique that creates an artificially induced environment that enable the permeabilization of the cell's membrane using electrostatic or electrodynamic pulses. The understanding of a very complex reaction such as electroporation is still not fully understood but researcher have theorized as to how bacterial transformation occurs. It is believed that the application of a sufficiently high electric field induces the molecular diffusion of the membrane's lipid bilayer, which allows the formation of pores in the surface of the cell. Diffusion, electrophoresis, electroosmosis, or a combination of these mechanisms then helps the transportation of the exogenous material through the accessible pores of the cell. Additional techniques have been explored for genetic engineering but for application in high throughput environments, current technologies are faced with some limitations in terms of applicability.

1.2: Methods to Genetically Transform Cells

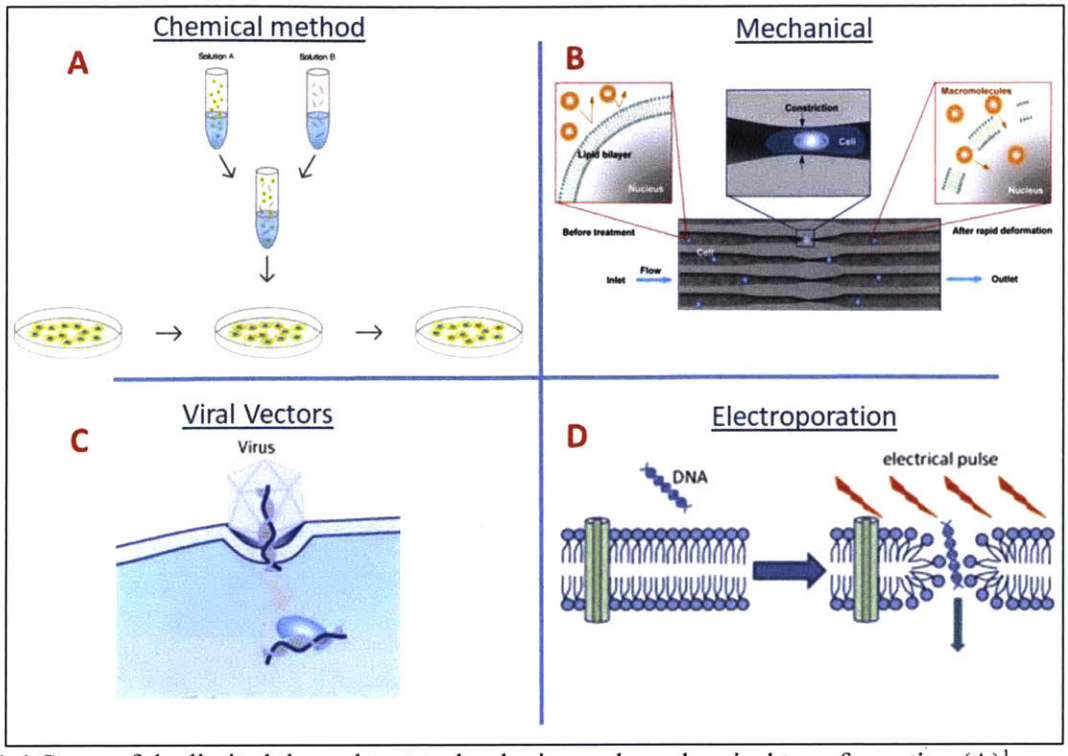

Figure 1-1 Some of the limited throughtput technologies such as chemical transformation (A)[1], mechanical induced transformation of cells (B)[2], the use of viral vectors (C)[3], and conventional cuvette electroporation (D)[4].

Figure 1-1 shows a diagram of some of the method used to transform cells. What is characteristic of these technologies is the fact that they are not currently high volume transformation techniques due a variety of factors, which will be discussed. Figure 1-1A shows chemical methodology of transformation of bacteria[1]. Chemical transformation or chemo-transformation is the process by which the addition of chemical compounds (most prominently divalent cation like magnesium, Mg^{+2} or calcium, Ca^{+2}) are added to chemo-competent cells. The addition of the chemicals/ions help to induce transformation of cells and allow for the insertion of exogenous material. Some type of shock mechanism, like a heat pulse, is also used to enhance transformation. The issue with chemo-transformation is that it is applicable to limit variety of specimens. In addition, in order to increase the efficiency some special processing steps maybe needed which can make the process strenuous, hence not adaptable for a high volume transformation environment.

Figure 1-1B shows mechanically induced method of transforming cells[2]. In the mechanical process, it hypothesized that a rapid deformation of the cell membrane induces pore formation and allow exogenous materials to be delivered to the cells. This methodology has been proven applicable to a variety of mammalian cell types such as immune cells and human fibroblast. The limitation of the technology comes about when the desired cell types are significantly smaller, in addition to hard to transform, as in the case of bacteria. Under the conditions to transform bacteria, it is required to have significantly smaller constrictions, which make the technique less practical because of the required dimensions. In addition, the technology has to be translated to a scalable platform in order to transform high volumes of cells. Therefore, the requirements for microfabrication must be removed in the construction of the device if the desire is to mass-produce the devices efficiently.

Figure 1-1C shows the use of viral vectors for transformation of cells[3]. Viral mediated transformation is the process of using a host viral vector to insert exogenous DNA in to cells. Viral mediated transformation is highly specific and extremely efficient. The issue with the methodology is the unforeseen reactions like cytotoxicity or immunogenicity, due to the presence of the vector used to transfer the exogenous material. In addition, viral vectors have a low packing capacity that limits the size of the base pair that can be inserted in vector, hence also the cells.

Figure 1-1D shows a schematic of electroporation in which an applied electric field distorts the cytoplasmic membrane[4]. The strand of DNA is inserted through the ephemeral pores in the cell's membrane, which is induced by the electrical pulse. The standard for industry and academia is the use of cuvettes in the electroporation process. In this situation, the current state of the art technology, the cuvettes, operate with volume of 50-200 μL. These minute volumes inhibit the rate transformation of cells, especially under condition when applied to low efficiency cells that are much harder to transform. The additional factors that makes the cuvette electroporation not suitable for high volume transformation is the fact that the technology has not yet been automated. Therefore, cuvettes electroporation has to be completed manually for every specimen. To enhance the efficiency, there has been numerous efforts to incorporate electroporation with microfluidics. Some of the prior technological achievements by other

scientists/engineers that have coupled microfluidic and electroporation are seen in Figure 1-2. This will be further discussed in detail in the next section.

1.3: Genetic Engineering with Microfluidic Devices

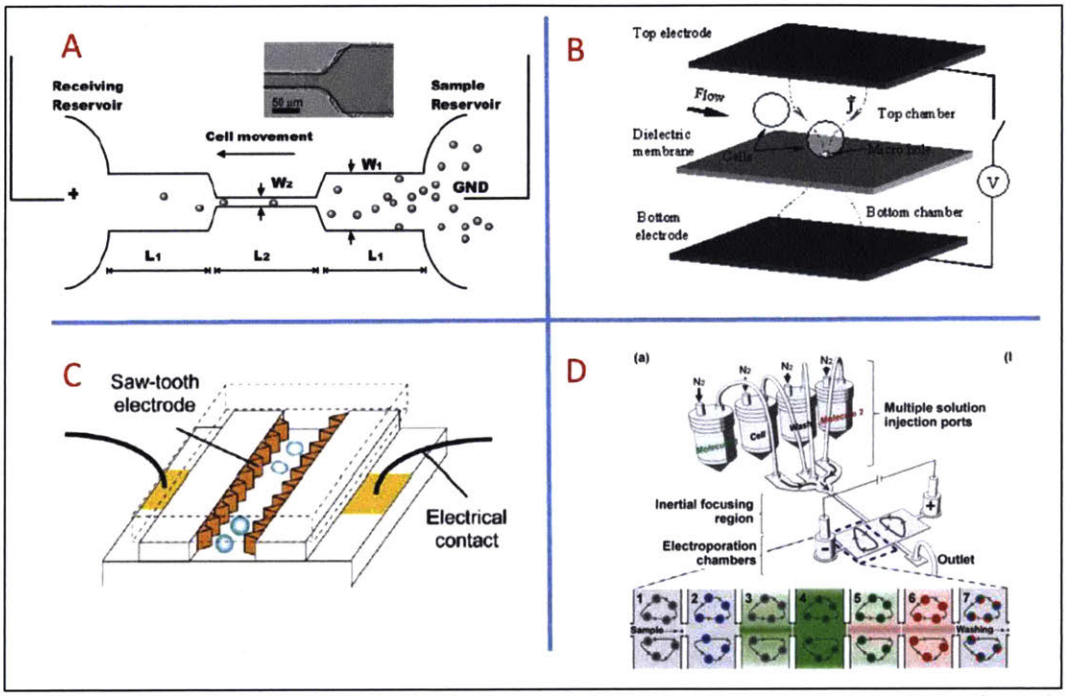

Figure 1-2: Selection of techniques that have incorporated microfluidic technology for cell manipulation. Image A shows a device used for lysis of bacterial cells by application of an electric field, which could also be used for electroporation to enhance their performance[5]. Image B shows a flow-through electroporation microfluidic device.[6] Image C is a microfluidic cell-lysing device that uses an applied electric field. Image D shows a mechanism that can sequentially insert DNA in a continuous manner by locally trapping cells with vortices[7].

Figure 1-2 is a list of various technology that have introduced a microfluidic platform to induce genetic transformation/transfection by application of a potential difference across a microfluidic channel. Figure 1-2A shows a device developed by Wand et al. that enables the amplification of an electric field due to the reduction of the cross sectional area of a microfluidic channel[5]. The device was used to investigate the regime at which lysis of bacterial cells can occur without the use of lytic agents. An alternative application of the device, as suggested by the authors, is electroporation of bacteria. Figure 1-2B show an excerpt from Huang et al. of a device fabricated to induce flow-through electroporation and single cell manipulation[6].

Figure 1-2C is an excerpt from research published by Lu et al[8]. The microfluidic device constructed by this group enabled researchers to determine the domain at which lysis of bacterial cells would occur. The authors used high frequency (1-100 kHz) alternating electrical potential differences across electrodes in a microfluidic channel. The electrodes were designed in a saw tooth manner to amplify the electric field at precise regions of the device. Figure 1-2D is an excerpt from Yun et al that used microfluidics to induce electroporation[7]. The device developed on the microfluidic platform allowed multiple molecules to electroporated in a sequential manner, in the same cell. The technology used a vortex assisted trapping mechanism within the electroporation regions. This enable Yun et al to sequential administer a variety of molecule to the cells in a precise manner. In addition to these, technology developed by Garcia et al, which incorporated geometric constraints in a microfluidic channel that creates a linearly increasing electric field exposure for bacteria[9]. All these technologies have advanced the genetic engineering microfluidic platforms. The technology developed by Garcia et al is the fundamental basis for the technological achievements discussed further in this thesis[9].

1.4: Overall Scope of the Thesis

The aim of this thesis is to introduce a scalable platform for electroporation that can be automated in order to increase the efficiency and rate of genetic engineering. The thesis focuses specifically on the application of microfluidics electroporation to enhance genetic transformation. The thesis also couples the microfluidic technology to 3D printing, which eases manufacturing requirements and removes the need for lithography. The chapters are partitioned in sequential manner to convey the design iteration, theoretical confirmation, and application of the device in the transformation of bacterial cells. The thesis then discusses some interesting and unforeseen correlation between the electrodes configuration and the possibility of optimizing the genetic engineering process in a microfluidic platform.

Chapter 2 introduces the design variations of both the microfluidic pipette tips and the flow through devices. Chapter 3 correlates the prior developed microfluidic chip technology and its connection to the

new devices that enable automated electroporation. Chapter 4 explores the performance of the microfluidic pipette tip as electroporation device. In addition, Chapter 4 also explores the application of variety of electrical waveforms, polarity and flow rate effects on the electroporation efficiency in the flow through devices and compares them to the current state of the art technology. Chapter 5 explores some unforeseen correlations that have significant impact on the electroporation efficiency. Parameters such as the electrode placement in the flow-through design and the total energy delivered per unit volume are explored. Chapter 6 is the culmination of the work completed. The chapter conveys the best conditions for the flow-through experiment (within the experimental domain). Chapter 6 elaborates on future work that might be completed in order to comprehend the impact of parameters in Chapter 5 and their correlation to the transformation efficiency.

Chapter 2

Prototyped Microfluidic Devices

2.1: Introduction

The prior chapter was short introduction to genetic transformation for prokaryotic cells (or transfection in the case of eukaryotes). The prior chapter's aim was to introduce current technologies that have potential for genetically engineer cells in industry and academia. Chapter 1 elaborates on the technical drawback/benefits of specific techniques and discusses why electroporation was undertaken in this thesis. Our group's currently technological advancement, the introduction of a flow-through microfluidic electroporation platform that applies a linearly increasing electric field, is introduced as a prominent technology that has significant applicability to enhancing genetic engineering at high volumes.

Chapter 2 focuses on the translation of the microfluidic chip platform to one that is more manufacturable. The term translation is used to describe the process of taking the polydimethylsiloxane (PDMS) microfluidic chip technology that was previously developed and applying it to a more scalable and manufacturable platform that relies less on clean room techniques. The difficulty that arises is the fact that the dimensions of the part are extremely hard to achieve if one chooses to circumvent the lithography process to manufacture the devices. Therefore, some adaptations to the design are introduced. The cross - sectional area of the constrictions are enlarged to approximately 400 μm diameter and the cross-sectional area is changed to a circular region, which will alters fluid dynamics. The goal of this chapter is elaborate on the design variations for continuous flow genetic engineering and the design of a discrete volume pipette tips that can be used for electroporation in a high volume genetic engineering environment. The term

'continuous flow genetic engineering' is used to describe an environment where biologist or engineers seek to transform large volumes (e.g. milliliters or more) of suspended cells in a continuous fashion. This is contrary to an environment, where genetic engineering is usually completed based on 100 μL, or less, which is more adaptable for the microfluidic pipette tips.

The chapter is structured in order to introduce the design variations of the prototypes by starting with the continuous flow devices and its benefits. Then chapter 2 introduces the translation of the technology to microfluidic pipette tips and discusses the benefits of the various designs. The end of the chapter shows the successful fabrication of working prototypes of both continuous flow and the microfluidic pipette tips fabricated with the use of stereolithographic 3D printing. The chapter ends with a summary of design variations to help the reader quickly assess the design benefits.

2.2: Continuous-Flow Device Designs

Rapid prototyping by 3D printing was used to manufacture the devices for application in the laboratory experiments. The translation of the technology was initiated by the development of continuous flow devices that obtained the predefined geometric constrictions within themselves. Then the design is extended to variations in the microfluidic pipette (MFP) tips that are compatible with conventional hand held pipettes. The first design iteration proceeds with the schematic depicted in Figure 2-1.

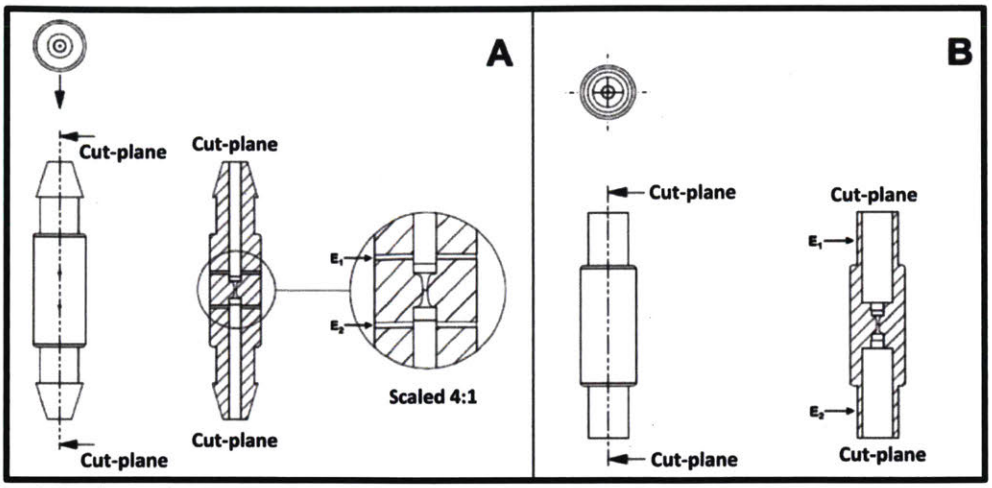

Figure 2-1: Flow-through designs for the electroporation process with the geometric constriction that enhances the electric field microorganisms will experience during the electroporation process. Image A shows a device with a barbed fitting at the tips and cylindrical electrodes perpendicular to the suspension's flow. The cut plane's surface exposes the electrode's (E1 and E2) placement and the constricted region. Image B depicted the design that relies on insertion of a dispensing needle in to the cavity of the device. The dispensing needles act as the electrodes when inserted in to the device (E1 and E2). The geometric constriction can also be observed along the cut plane of image B.

Figure 2-1 shows the flow-through devices that are used in some of the experiments conducted in this study. These devices were designed for electroporation of prokaryotic microorganisms in a continuously flowing manner. In addition, the devices were designed in order to transform significantly large volumes of suspended microorganisms. With these devices, the ability to transform numerous liters of suspended cells is now easily achieved in comparison to doing single experiments at with cuvettes. Continuous transformation could be achieved with the use of a peristaltic pump, which removes the volume restrictions. The device with barbed fittings, Figure 2-1A, is designed to be used with tubing that are biologically compactible with the particular cells being transformed. In our experiment, we have used Tygon Tubing®, which has minimal chemical reactivity with *Escherichia coli*. Figure 2-1A has a transverse circular electrodes (E1 and E2) made of stainless steel or platinum as seen in the 4:1 scaled inset image. The constriction designed in the flow-through devices has the same cross-sectional area variation along the rotational axis as those seen in the assay devices developed by Garcia et.al[9]. Figure 2-1B, shows the flow-through device with an insertion region for the dispensing needles. These flow-through devices were designed to accommodate dispensing needles that seal by a compression fitting between the polymer of the device and the stainless steel dispensing tips. The devices allow the dispensing needles' tip to act as

electrodes in the electroporation process. The configuration seen in Figure 2-1B changes the electrodes design to one that is axially symmetric (E1 and E2 Figure 2-1B.) which provide a more uniform electric field over the cells.

2.3: Variation of the Microfluidic Pipette Tips

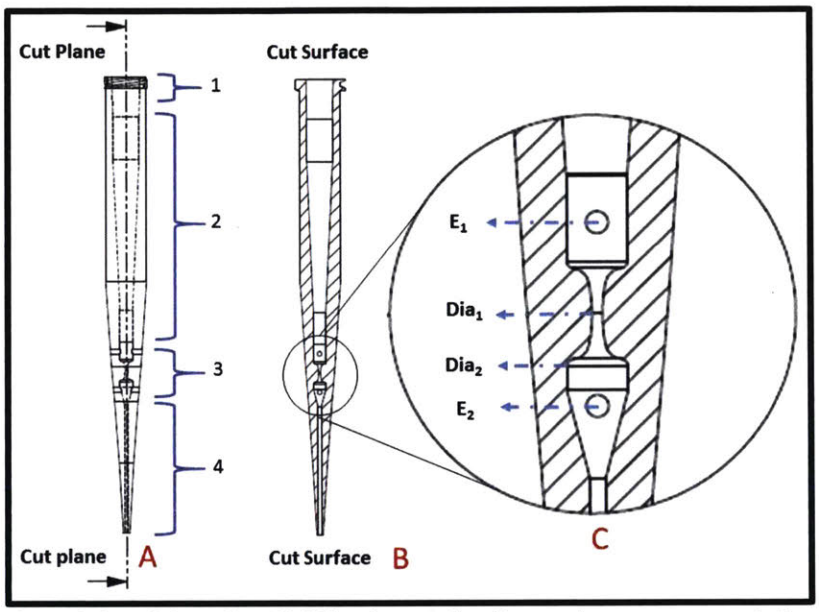

Figure 2-2: A depiction of the of the microfluidic pipette tips for use in an automated electroporation process for microorganism. The device has regions to insert cylindrical wire electrodes. The device is designed to aspirate and dispense precise volumes of suspensions. Region 1 is designed with a luer lock fitting in order to connect the device to a syringe. Region 2 acts as a flow channel and temporary reservoir. Region 3 is the geometrically designed constriction of the device. Region 4 is the liquid interface area. Schematic A is the full depiction of the device, schematic B is the cut plane, and Schematic C is the magnified illustration of region 3. Schematic C shows more detail of the constriction parameters such as the minimum diameter Dia1, maximum diameter Dia2, and electrode placement.

Figure 2-2, is an illustration of the device created to enable the automatic transformation of microorganisms by electroporation. This configuration enables the individual pipettes to aspirate and dispense precise volumes of the microorganism suspension for the electroporation process with use of a connection to the female luer lock (region 1). Alternative design configurations of the microfluidic pipette tips enable the use of different designs at region 1 that allow for quick-connects, interference-fittings, luer slips, and other connectors. The ability to connect the microfluidic pipette tips to a variety of connections enables more method of controlling the fluid flow with various apparatuses. In region 2 of the MFP tip, the

tip act as a reservoir for the suspended cells. First, the cell are aspirated above both electrode before the electric pulse is applied in region 2. The suspension is then dispensed at a precise rate that is designed for the particular microorganism. The pulse is triggered when the flow front of the suspension makes contact with the bottom electrodes (when both electrodes are immersed in the fluid) which reduces the dielectric break down and arcing in the cavity of MFP tip. Region 3 contains the geometrically design constriction that varies along the fluids path. Region 3 also contains the electrodes of the device. The electrodes are cylindrical wires that are placed transverse to the fluid flow during electroporation. Region 4 is a tapered design that allows for minimal surface interaction with the suspension. This enable better aspiration, dispensing, and more precise control over the quantities of fluids that are used during electroporation. Figure 2-2A, show the full design with designated regions of the device. Figure 2-2B shows the cross-section along the symmetric axis of the device. Figure 2-2C, shows the magnified image of the cross-section with depiction of the electrodes (E_1 and E_2) and Diameters (Dia1 and Dia2).

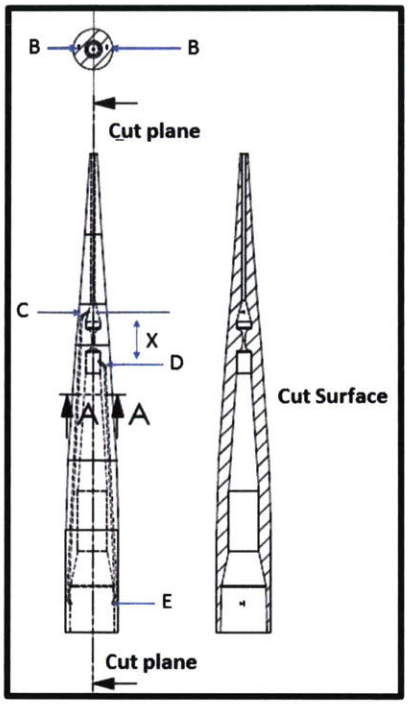

Figure 2-3: Imbedded electrode design for the MFP tips. Line A is plane that show the projection of the cross section above at section B. Section B, the electrode are incase in the polymer or the walls of the MFP tips. The electrodes in this design are separated across the axis of the device. C and D are the locations at which the negative and positive electrodes interact with the flowing suspension of microorganism. E is the location of the electrodes contacts. X is the distance between electrodes.

Figure 2-3 introduces an alternative design of the MFP tip where the electrodes are embedded in the polymer that forms the device during an injection molding process. Figure 2-3 show the labeled schematic with specific areas of interest. Region A in Figure 2-3 is the region where the cross-section can be observed. Region B in the schematic indicates the part of the electrodes encapsulated in the particular polymer chosen for the design. Designated regions C and D are the part of electrode that are in direct contact with the suspension during the electroporation process. Electrodes are supplied with the potential difference at region E when the device is connected to a manifold connected to a control system. The schematic also shows the cut surface or cross-section of the device, which is similar to previous designs.

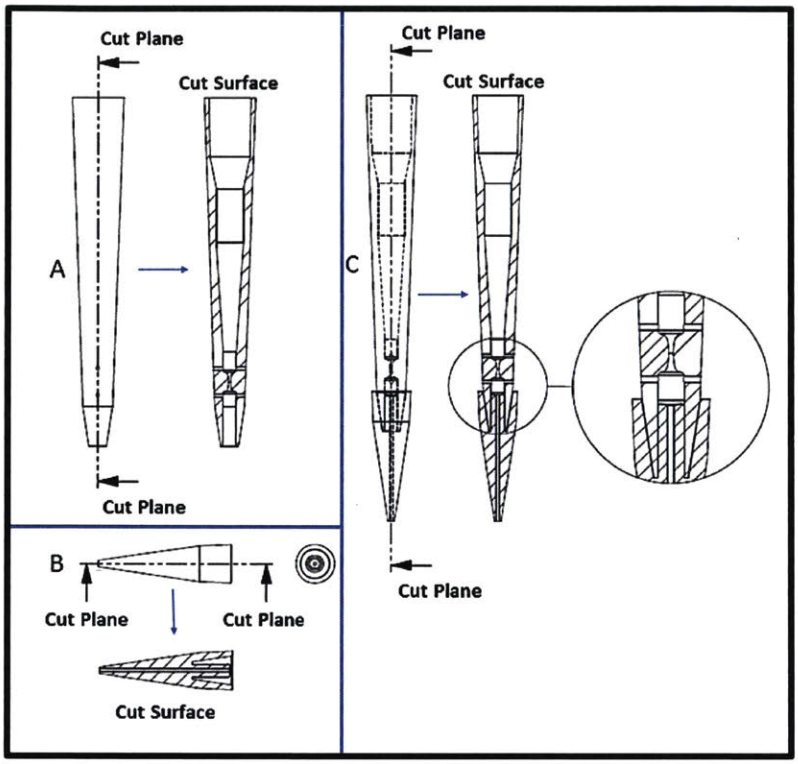

Figure 2-4: Microfluidic pipette tips that utilize a modular approach in its construction. The device is defined in a modular manner in order to increase the feasibility of injection molding by production. Section A shows the reservior of the device and it crossectional area which include the constriction region. Section B is the cap and it crossectional area. Section C shows the method by which the parts intereference.

Figure 2-4 introduces the modular design of the MFP tips. The design portrayed within this figure introduces a more easily manufactured part for a high volume-manufacturing environment. The design follows injection-molding rules: corrected draft angles for easy release, uniform thickness to reduced deformation and warping. The design is split into two regions, section A and section B. These regions can be easily injection molded due to the lack of the designed constriction that leads to encapsulation of the insertion pin in the injection molding process. Section A is the reservoir cavity that contain the specified constriction region of the device that induces the electric field amplification for a particular species of cells. Section A also contains the region of insertion for the manifold in order to introduce a compression or interference fit for a vacuum seal. This upper-region/reservoir of the modular design is energized with wire electrodes that are introduced after production of the part. Section A also shows the cross section of the reservoir region of the modular design. In Figure 2-4B, the cap can be observed for the modular design. This region does not induce any cross sectional modification that amplify the electric field. This region

enables precise aspiration of the 100 microliters of suspension. Figure 2-4C show the connection of the modular design during operation. The cap and reservoir are secured by compression/interference fitting. This design is specifically introduced because it could be undertaken without the need for prior additional construction at a manufacturing facility, which reduce the overall cost.

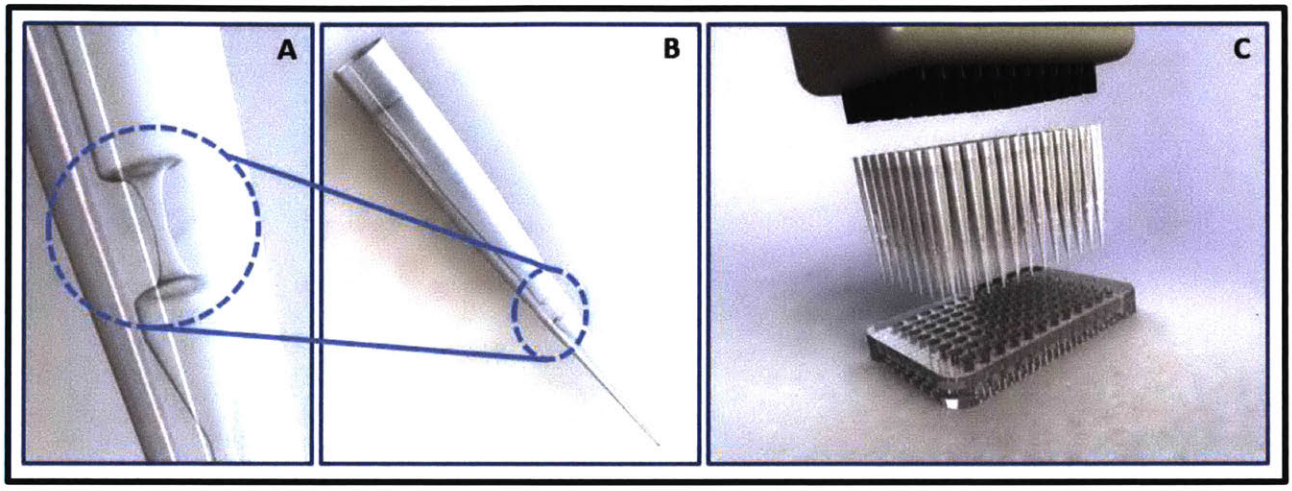

Figure 2-5: 3D rendered model of the MFPs that were used in the pipette electroporation experiments. Section A is the enhanced view of the constriction, which can be observed through the polymer. Section B show shows the entire device with the interference or compression fitting at the base of the MFP. Section C, shows the prospective view of 96 MFP tips being used simultaneously with a liquid handling manifold and a 96 well plate, which would significantly enhance the rate of genetic engineering microorganisms.

Figure 2-5 shows the rendered model of the prototype devices and its incorporation into a scalable liquid handling system. Figure 2-5A and Figure 2-5B show depictions of the prototyped models used for both hand held pipettes and the liquid handling manifolds. Figure 2-5C shows the future perspective a of a high throughput platform for genetic engineering. The use of the tips and liquid handling manifold enable 96 electroporation experiments simultaneously.

2.4: Fabricated Prototypes

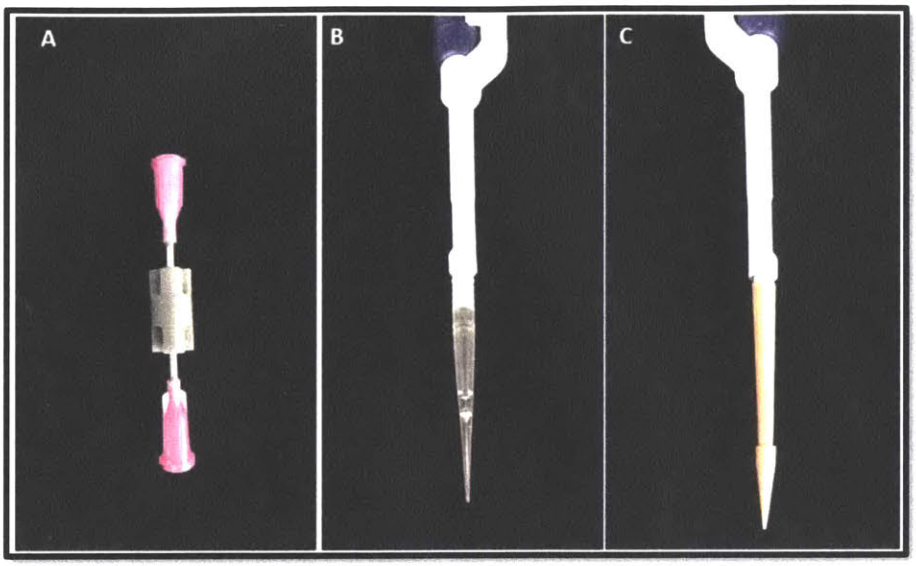

Figure 2-6: Stereolithographic printed microfluidic devices. Section A is a depiction of the flow-through devices, similar to the schematics shown in Figure 2-1A. Section B, shows the 3D printed version of the seen in Figure 2-5. Section C shows the depiction of the modular design of the MFP tip connect to a manual pipette tip. This design is similar to the schematic shown in Figure 2-4.

Figure 2-6 show a variety of 3D printed models and their final configuration. Figure 2-6A shows one of the variations of the continuous flow devices with luer lock dispensing needles inserted into the 3D printed device. Figure 2-6A is similar to that depicted in Figure 2-1B. In this variation of the flow-through device, the external power supply contacts the top and bottom stainless steel metals of the dispensing needles and they act as electrodes. In Figure 2-6B, the device shows the MFP tip's variation for the flow-through designs. The design variation in Figure 2-5B is similar to that in Figure 2-6B. The MFP tip is inserted on to a Rainin 200 μL single channel manual pipette for illustrations. Figure 2-6C shows the 3D printed modular design that is similar to Figure 2-4. The reservoir of the design is connected to both the cap and a Rainin 200 μL single channel manual pipette. The method of 3D printing the MFP pipette tips and the continuous flow-through devices has shown to be successful. The major parameters of the critical dimension (the constricted region) and concerns about interference fitting have been solved through repeated design variations and testing during the manufacturing.

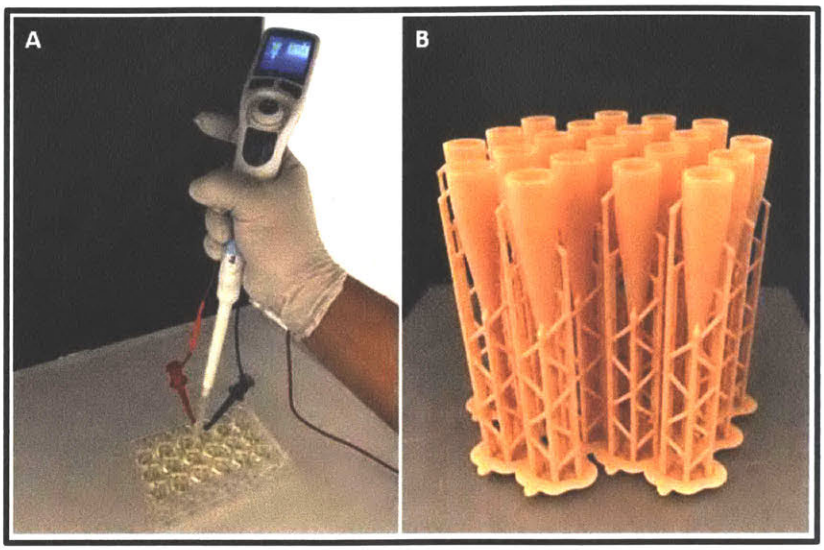

Figure 2-7: Section A shows an experimentalist conducting an electroporation experiment by applying an external potentials difference with the use of a power supply. Section B show the scalable production of the variation of the microfluidic devices. (Note: section B's design schematic are not listed in the design variations.)

Figure 2-7A shows the use of the MFP tips in operation during the electroporation experiment. Wire stainless steel electrodes are inserted into the MFP tips. The wires connect to the external power supply in order to deliver the pulse during the electroporation process. The electrodes, red and black attachment on the MFP tip in section A, supply an external potential difference. The MFP tip is connects to an automatic dispensing pipette, which controls the flow rates precisely in the experiments. Figure 2-7B shows a cluster of MFP tips printed from biocompatible dental resin using a Formlabs Form 2 desktop 3D printer that uses stereo lithography (SLA) technology. Rapid prototyping of the microfluidic device enhances the flexibility of the design at low cost. The designs are usually constrained by the desired critical dimension (constriction size) versus those that the system is capable of producing. Some aspect of the critical dimensions in the MFP tips, such as the cross sectional area of the constriction, have increased in order to prevent clogging of the constriction.

Overall, successful translation of the PDMS microfluidic chips has been demonstrated concerning manufacturability. Proceeding chapters will elaborate on their capability to genetically engineer bacteria and test the device functionality. To investigate the performance of the design iterations, simulations have been completed to confirm the design variation are still capable of replicating the same electric fields as in

the microfluidic chips. The next section will elaborate on the findings. To assess the device variations and their overall benefits, Table 1 is added as a quick reference to distinguish between the devices.

Table 1: Benefits of Model Variations

Device Figure	***Model Type***	***Benefits***
Figure 2-1A	Continuous-flow	• Continuous electroporation of large volumes • Electrode inserts for material specific interaction
Figure 2-1B	Continuous-flow	• Continuous electroporation of large volumes • Dispensing needle used as electrode • Injection moldable
Figure 2-2	MFP tips	• µL volume control • Adaptable to syringes • Electrode insert
Figure 2-3	MFP tips	• Adaptable to liquid handling platform • µL volume control • Embedded electrodes-compact design
Figure 2-4	MFP tips	• Adaptable to liquid handling platform • µL volume control • Modular Design – Injection moldable

Chapter 3

Flow-Through Electroporation in Microfluidics

3.1: Introduction

The prior chapter illustrates the designs of the microfluidic devices that were developed to for flow-through electroporation in a continuous manner. Chapter 2 also introduced the MFP tips that enable electroporation in an automated liquid handling platform. The (MFP tips and Continuous flow) devices all contain the same geometric constrictions, which affect the electric fields experienced by the specimens as it flows through the device.

Chapter 3 focuses on confirming the translation of the constriction that was previously developed for use with the microfluidic chips. The chapter also compares them to the newly developed prototypes. In the past, the microfluidic chips' constricted regions were prismatic in form. The MFP tips and continuous flow devices have a circular constriction. This chapter seeks to confirmation the designed electric field distribution along the dimension of the prototyped device. In addition, the need to understand the flow rates versus exposure to the amplified electric field needs to be understood.

In Chapter 3, simulation of both the microfluidic chips and the MFP tips/continuous flow through devices are presented. The prototypes developed have similar electric field distribution even though the geometric configuration between the microfluidic chip and MFP tips are different within the constricted

region. Simulation of the electric field distribution in combination to the fluid velocity also gives insight into the impulse experience by the cell as a function of the flow velocity.

3.2: Microfluidic Chip Electric Field Distribution in Bilateral Constriction

Electroporation of *E. coli* Dh10 beta was completed with the use of microfluidic pipette tips in order to investigate the efficacy of the technological translation from laboratory PDMS microfluidic chips. To begin the investigation and compare the microfluidic chips versus the performance of the microfluidic pipette tips, COMSOL Multiphysics® simulations were completed to ensure that the linear electric fields that were designed in the microfluidic chips could be replicated in the MFP tips. An excerpt of prior work describing the electric field along the microfluidic chips can be seen in Figure 3-1[9].

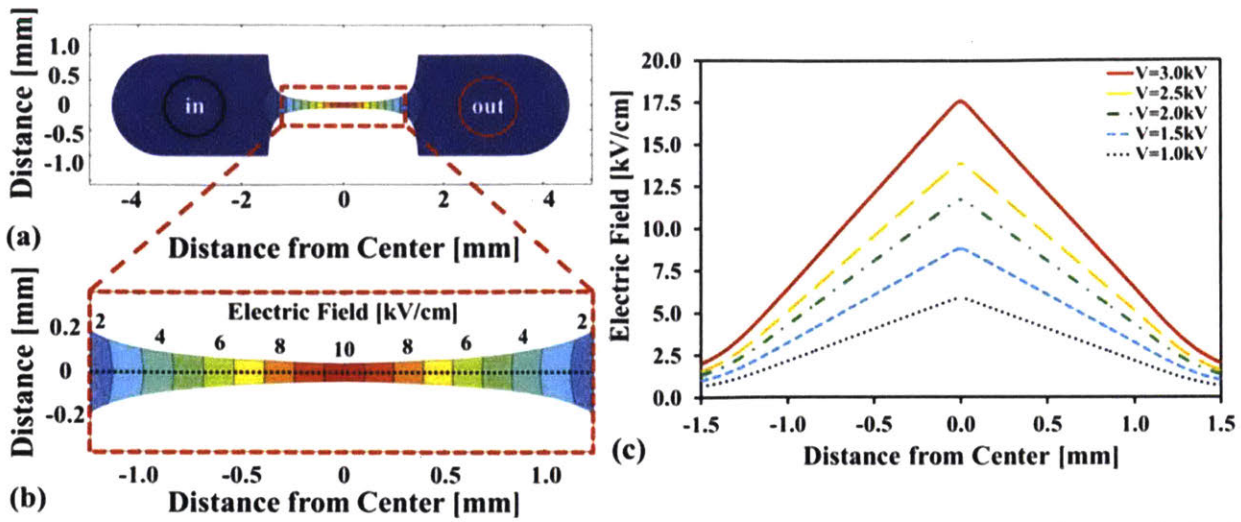

Figure 3-1: The electric distribution field inside the microfluidic devices that were design by Garcia, P. A. et al[9]. Section (a) shows the distribution of the electric field along the microfluidic device and also the inlet and outlet for the suspension. Section (b) shows a magnified image of the constriction's amplification of the electric field in the microfluidic device. Section (c) shows a plot of the constriction's electric field distribution along the centerline of the channel. By changing the applied voltage or the cross sectional area's dimension, one can control the maximum electric field and the rate at which the microorganism experiences the applied electric field.

Figure 3-1 is an excerpt from previously published article within the Laboratory for Energy and Microsystems Innovation (LEMI) at MIT, which is the predecessor of this work. In Figure 3-1, the linearly increasing electric field designed in the microfluidic chips can be observed. Figure 3-1 (a) show the electric field distribution along the centerline or the longitudinal axis of symmetric in the microfluidic chip. Figure 3-1(b) shows the magnification of the constricted region to illustrate the spatially incremental increase in electric field along the device. Figure 3-1(c) shows the electric field distribution along the longitudinal axis of the microfluidic chip as a function of various potentials at the electrodes. Figure 3-1(c) shows the linear increase in the electric field potential as a function of distance. In addition, Figure 3-1(c) also shows the amplification of the electric field and the maximum electric field that the flow suspension experience at particular potential difference ranging from 1 kV to 3 kV. For example with an applied voltage of 3 kV, the maximum electric field is approximately 17.5 kV/cm experienced by the suspended microorganism during the electroporation process. The amplification of the electric field reduces the needed potential difference and increases the electroporation efficiency. We extended this theoretical analysis with COMSOL

Multiphysics® to investigate our new circular design of the constriction region in the microfluidic pipette tips.

3.3: Electric Field Distribution in Prototypes

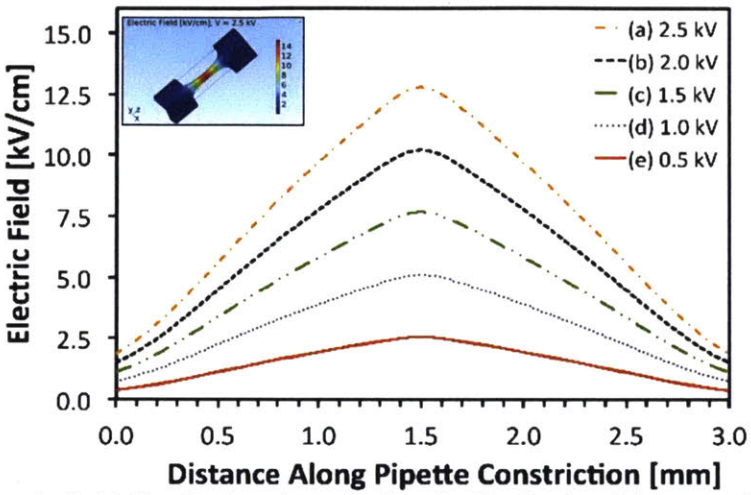

Figure 3-2: Spatial electric field distribution along the longitudinal axis of the constriction within the MFP tips at variety of voltage ranging from 0.5 to 2.5 kV. This confirms the spatial distribution similarity to that of the microfluidic devices build by Garcia, P. A. et al[9]. The inset image is a 3D spatial distribution of the simulated electric field within the constricted geometry of the MFP tips, which was completed in COMSOL Multiphysics®.

Figure 3-2 shows the spatial distribution of the electrified in kV/cm along the center of the constricted region of the MFP tip. Figure 3-2 also shows an inset image of the spatial distribution in the investigated design of the constricted region within the microfluidic device. The COMSOL Multiphysics® simulation shows that the design of the MFP tip's constriction successfully translates the microfluidic PDMS chip's constriction to provide a similar configuration of a linearly increasing electric field along the central axis of the device. Figure 3-2 shows the simulated electric field vs. the distance along the centerline of the pipette's constriction. The supplied potential difference in the design varies form 0.5 kV to 2.5 kV and the peak amplification of the electric field varies from 2.5-12.5 kV/cm. The specified design amplification in this design of the constriction is 5X. Therefore, the magnitude of the applied voltage to generate the peak electric field is five times the applied potential difference. Therefore, a 2.5 kV potential difference generates a 12.5 kV/cm peak electric field at the center of the constriction. The simulation has

been extended to investigate the electric fields that are observed as a function of the flow rate of the suspension in the microfluidic pipette tips.

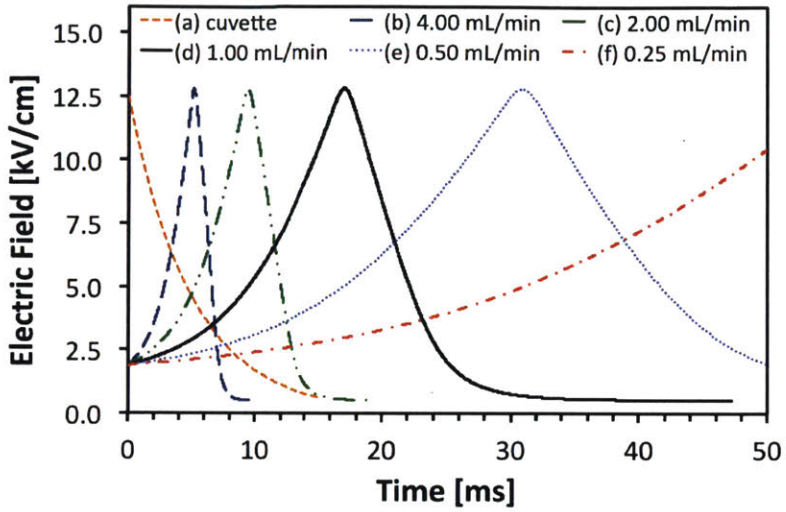

Figure 3-3: Simulated electric field as a function of time. The microorganism experiences the simulated electric field during the flow-through electroporation experiments in the microfluidic pipette tips. A constant 2.5 kV potential difference has been applied to the electrodes during the simulation. The simulated flow rates range from 0.25-2 mL/min. The cuvettes electroporation electric field, a decay function, is also expressed in the figure as a basis for comparison.

A strongly coupled correlation to transformation efficiency is the velocity/volumetric flow rate of the suspension used during the flow-through electroporation experiment. In Figure 3-3, the electric field experienced by the microorganism as a function of time at discrete flowrates are plotted from the COMSOL Multiphysics® simulations. The peak electric fields experienced by the cells remain constant throughout all of the simulated flowrates, as expected. The residence time experienced is significantly different between flow rates, which affects the overall electric field exposure of the cells. The residency time is the time span at which the cell is exposed to the amplified electric field. The residency time is the last data point collected on the plot for each particular flow rate. For example, at 2.00 mL/min the residence for this simulation is approximately 19 ms. This residence time is correlated to the amount of energy delivered to the microorganism throughout the experiment. As the volumetric flow rate increases, the residence time decreases in the MFP tips. The plot in Figure 3-3 includes the electric produced by the cuvette system, which is described by a decay function. The decay function has a time constant of 1.5 ms and an applied peak electric field of 12.5 kV/cm. (The same as the peak electric fields were used for the MFP tips). For

the cuvettes, the residence time is approximately 16 ms. To gain a better understanding of the electric field exposure as a function of time and the cumulative effects we have plotted the normalized residence time versus the electric field experienced by the suspension of microorganisms.

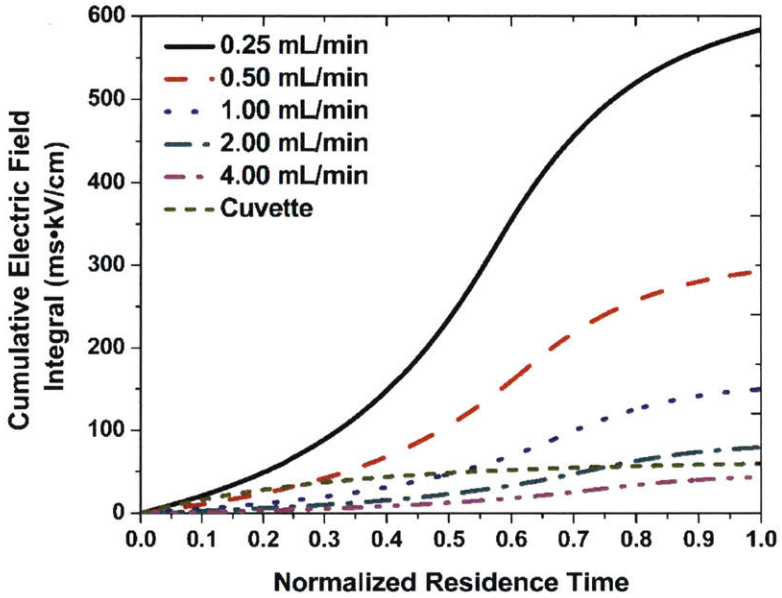

Figure 3-4: Cumulative electric field versus the normalized residence time and the volumetric flowrate of the suspended cells as they move throughout the MFP tips. The applied potential difference is 2.5 kV throughout the simulation. As can be seen form the plot, the slower flowrates show significantly higher level of cumulative exposure to the cell in comparison to the decay function.

The plot in Figure 3-4 shows the cumulative electric field integral as a function of the normalized residence time. The cumulative electric field integral is the integrated electric field exposure over the residence time of the microorganism. From the figure, at 0.25 mL/min, the integrated electric field integral is approximately 580 kV·ms/cm. The cuvette's cumulative integral of electric field is only 60 kV·ms/cm. Comparing these two experiments, there is approximately a 10 times increase in energy that the cell experience throughout the electroporation process because of its flows at 0.25 mL/min. At a flowrate of 4 mL/min, the cumulative electrified exposure is approximately 43 kV·ms/cm. Which is less energy delivered for the same suspension. The interesting aspect is how the flow rate parameter affects the transformation efficiency during the electroporation experiment. Therefore, to investigate the flow rate correlation to transformation efficiency, an experiment that varies the flowrate and the applied voltages was conducted with the use of *E. coli* DH10β.

Flow-Through Electroporation in MicrofluidicsChapter 3 emphasizes the distribution of the electric field along the central axis of both the microfluidic chips and the MFP pipette tips. Overall, simulations have shown that the geometric design of the constriction are similar in terms of electric field distribution, which means that the devices provide the same electric field impulse to the cells. The flow rates used in the simulations show that they are significantly important parameters because of the impulse experienced by the cells. This correlation of electric field exposure versus flow rate will be discuss further in Chapter 5, where we considered experimental results for the transformation efficiency of the cells. The simulation of the electric fields was successful and the next chapter seeks to confirm the devices' transformation efficiency experimentally.

Chapter 4

Electroporation Experiments

4.1: Introduction:

In the prior chapter, the electric field distribution along the central axis of the MFP tips and the electric field exposure versus time (cumulative electric field) were the most important aspects. Simulations in COMSOL® confirmed the similarities between the electric field distribution of the prior chip technology and the prototyped devices. The primary focus of Chapter 4 is to introduce the experimental technique used to quantify the transformation efficiency and test the efficacy of the prototyped design. Chapter 4 initially describes the experimental procedures for the cell preparation, and then the chapter describes the experimental processes for the flow-through electroporation conducted. Experimental results for the transformation efficiency versus flowrate and applied voltages are compiled. There is a slight shift in moment as one proceeds throughout the chapter. Variation in the waveform and the polarity as experimental parameters are introduced. These experiments are mainly conducted in the straight channel PDMS microfluidic chips. This shift from the use of MFP tip is because it is hypothesized that these parameters may have significant effect on the transformation efficiency and a basis is needed for comparison, therefore, prior technology is used. Throughout the Chapter 4, data supports the fact that the MFP tips outperform the cuvette technology. Which indicates that the technology introduced in this thesis can sufficiently replace the current start of the art without loss in performance. In addition, it is observe that factors like the polarity and waveform play a tremendous role in the transformation efficiency.

4.2: Cell Culture Preparation

A single colony of *Escherichia coli (E. coli)* DH10β was removed stock petri dished using an inoculation loop to ensure that all bacteria replicated were from the same mother cell to ensure genetic uniformity. This Stock petri dish was created from a purchased batch DH10β Escherichia that was maintained at minus 80 degrees Celsius (C), and then plated onto the surface of 16 ml of Luria-Bertani (LB) medium plus agar in a 60 mm x 15 mm VWR international polystyrene petri dish. The stock colonies were streaked onto the surface of agar plates and stored at 20 C. To start the *E. coli* culture, a single colony was removed from the stock agar plates using a sterile inoculation loop. The colony is then transferred to a 5 mL cell culture tube that contains 3 mL of sterilized LB. The LB media was prepared with the use of BD Difco™ Dehydrated Culture Media at a concentration of 25 g/L of de-ionized water. The LB mixture was autoclaved for sterilization. The 3 ml of suspended cells were shaken at rate of 250 revolution per minute (rpm) at 37°C overnight (approximately 10-16 hrs.).

Electrocompetent *E. coli* Preparation

After the incubation period overnight, 1.25 mL of the cell culture is transferred to a 500 mL Erlenmeyer flask that contains 200 mL of sterilized LB. The cell culture is then incubated for approximately 3.5 hrs or until the cell culture has reach mid log phase (OD_{600}=0.5). After the correct OD_{600} is achieved, the sample is centrifuged in order to concentrate the *E. coli*. The cell culture is transferred into six 50 mL centrifuge tubes with equivalent volume (~33mL). The first centrifugation occurs at 3500 rpm for 10 minutes at 4 C. The LB suspension is removed after the cell culture is centrifuged and the plated bacteria is re-suspended with a 10% w/w Glycerol to water mixture that was stored at 4 C. The cells are then re-suspended with 1 mL of 10% Glycerol for each of the six centrifugation tubes. The 1 mL of 10% glycerol and *E. coli* is then transfer to 1.5 mL Eppendorf tube in order to be centrifuged again in a series of washes using 10% Glycerol. The sample is centrifuged at 8000 RPM for 5 minutes at 4 C. After the 5-minute interval for the centrifugation, the supernatant is disposed and the pelleted bacteria are re-suspended with 10% glycerol. The rinsing of the sample with the use of 10% glycerol is repeated 3 times. After the last wash of the *E. coli*, the supernatant is again disposed. The pelleted cells are re-suspended in a total of 1 mL

of 10% Glycerol. The OD_{600} is measured and once the concentration of the cells is determined, the volume is diluted to the desired operating concentration for the electroporation experiment.

4.3: Electroporation Procedure for Flow-Through Experiments

Cuvette electroporation is done with 2 mm gap electroporation cuvettes form VWR international. The Standard operating procedures were followed for electroporation of *E. coli* during the experiments. 200 µL of the electro-competent cell in 10% glycerol were pipetted into the cuvettes. (The cuvette were stored in an ice bucket before the procedure in order to increase cell electroporation viability). After addition of the cells, the cuvettes are then inserted in the Micropulser™ Electroporator and the desired pulse is triggered to deliver the electric field. The cuvettes are quickly removed after the pulse delivery and 800 µL of LB is added to the cuvettes in order to start the recovery process.

For the flow-through experiments, 100 µL of electro-competent cells are allocated to each experiment. For the electroporation with the use of the microfluidic chips, the suspension are aspirated into Tygon® tubing of specified internal diameter (1/16 inch) using a syringe. The tubing is not removed from on the syringe. The syringe is then places inside a syringe pump in order to control the flow rate precisely during the experiments. The alternative end of the tubing that contains the electro-competent has a stainless steel tube, which has an external diameter that matches the internal diameter of the Tygon® tubing. This added stainless steel tube acts as an electrode during the experiment. Two stainless steel tubes are used to complete the circuit during the experiment. One of the electrodes is placed at the inlet and the other at the outlet of the microfluidic chips so that the cells can traverse the constricted region and be collected afterwards. The cells are pressure driven from the tubing to the inlet of the PDMS microfluidic chips were and electric pulse is applied between the inlet and outlet of the microfluidic chip. The sample is collected afterwards into 900 µL of LB to initiate the recovery process.

Electroporation in the MFP tip are similar to that of the flow-through experiment in the PDMS microfluidic chips. The MFP tips are connected to syringe pumps for precise control over the volumetric flowrate. MFP tips have two stainless steel wire electrodes exposed to the 100 μL of electro-competent cells as they flow through the constriction of the device. As the sample leaves the MFP tip it is collected into a well that contains 900μL of LB media that initiates the recovery protocol.

During the recovery, the sample is incubated in the LB after the electroporation process for 1 hr. After the 1 hr time has elapsed, the sample is then diluted at a ratio of 10,000 time per OD_{600}. The samples are diluted with the use of de-ionized water or cell-culture-grade water purchased from VWR. After the dilution, 100 μl of the sample is then plated onto an Agar+Ampicillin plate in order screen for successfully transformed cells. The plates are prepared with the use of Bacto Agar (20 g/L, Difco LB Broth (25 g/L), and ampicillin at a concentration of 50 μg/mL. The plate with the electroporated specimens are then incubated at 37°C for approximately 16 hrs or until a preferred diameter of the individual colonies are achieved for easy quantification. The individual colonies are counted with the use of a colony counting software.

4.4: Electroporation in Microfluidic Pipette Tips

Table 2: Parameter for the flow-through experiment using the geometrically configured 3D printed microfluidic pipette tips.

Parameters	***Values***
Flowrate(mL/min)	0.25, 0.5, 1,2 and 4
OD_{600}	10
Conductivity of cells with DNA	Not Measured
Waveform used	5ms pulses (or 95% duty cycle)
Control cuvettes parameters	1.25kV, 1.75kV and 2.5kV; τ=1.5ms
Voltage applied (kV)	0.5,1, 1.5, 2.0 and 2.5
Devices	Microfluidic Pipette Tips

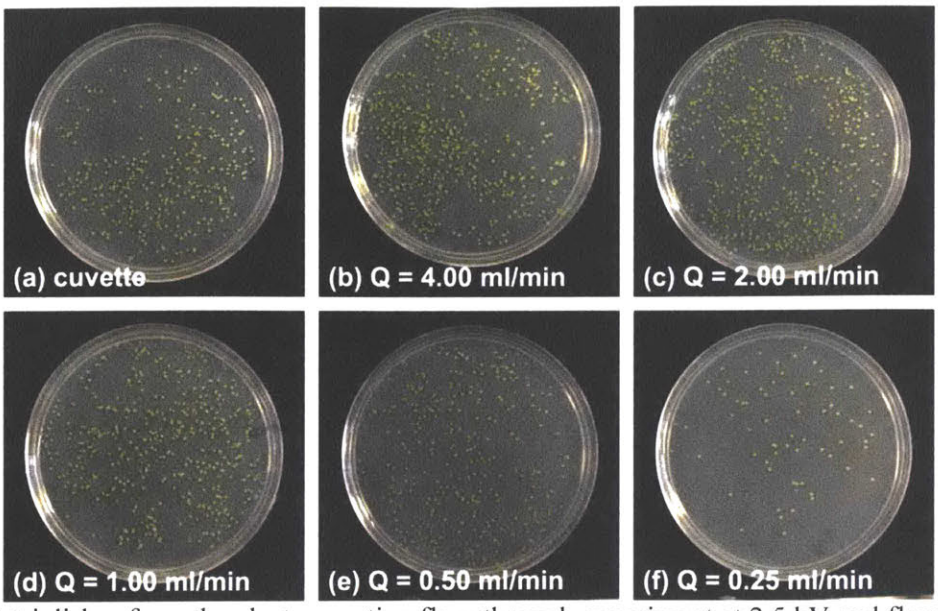

Figure 4-1: Petri dishes from the electroporation flow-through experiment at 2.5 kV and flow rate of 0.25-4 ml/min of *E. coli* DH10β. The pulse used in the experiment was 5 ms (or 95% duty cycle). Overall higher flow rates are more desirable for the electroporation experiment as seen by the increase in the density of fluorescent colonies and hence an increase in transformation efficiency.

The experimental parameters are listed in Table 2 for the flow-through experiment using the microfluidic pipette tips. The applied voltage range during the experiment was 0.5-2.5 kV (in increments of 0.5 kV) and flow rates of 0.25 ml/min to 4 ml/min (doubled at each increment). The experiment was completed at OD_{600} equivalent to 10. After the experiment is completed, the concentration of the cell is diluted 10,000X per OD_{600} in order to quantify the number of cells that are successfully transformed during the electroporation process. Figure 4-1 (a-f) shows the petri dishes from the electroporation process using the microfluidic pipette tips and the petri dishes obtained from using the cuvettes as a reference. The petri dishes show the colony form unit (CFU) of *E. coli* DH10β that have successful been transformed during the electroporation process. The DH10β cells do not natively possess the ampicillin resistance nor the ability to fluoresce green. Therefore, the cell's presence on the surface of the agar/ampicillin petri dish confirms successful transformation by electroporation using the MFP tip. From Figure 4-1, the correlation that is discerned is that as the flow rate increases in the device, there is an increased in the transformation efficiency of the MFP tips. The formula for the transformation efficiency:

$$\text{Transformation Efficiency} = \frac{\#\text{ of CFU}}{\mu g_{\text{DNA used}}} \times \frac{\text{volume transformed}}{\text{volume plated}} \times \text{plating factor}$$

The overall experimental parameters variation, volumetric flowrate, and applied voltage versus efficiency is plotted in Figure 4-2

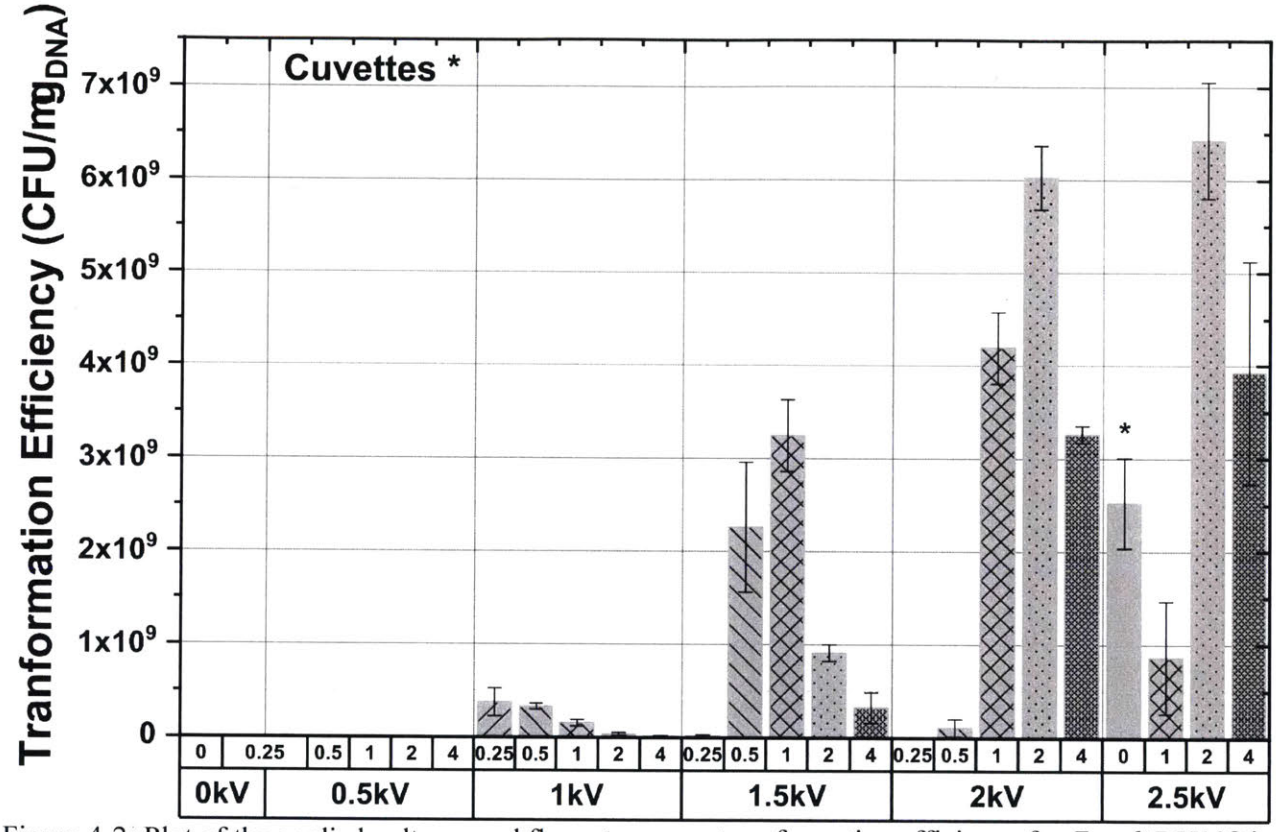

Figure 4-2: Plot of the applied voltages and flowrate versus transformation efficiency for *E. coli* DH10β in the MFP tip devices. As can be observed the highest transformation efficiency is observed at a combination of 2.00 mL/min and applied voltage of 2.5 kV. For the Higher applied voltage of 2.5 kV, flow rate of 0.25 ml/min and 0.5 ml/min were not used in the experiment due to overheating of the samples during the electroporation process. Overall, the MFP tip has outperformed the cuvettes with the application of less potential differences.

Figure 4-2 shows the overall transformation efficiency of each individual experiment conducted in the MFP tips. The MFP tip were fabricated using an EMBER® 3D printer. The MFP tip contains a 3.0 mm length constriction that decreases bilaterally from 2,050 μm to 400 μm in diameter at the smallest region of the constriction. The plot shows the applied voltage versus the transformation efficiency of *E. coli* DH10β at each flowrate and the cuvettes' performance as a reference. The maximum transformation efficiency throughout the experiment was observed at 2.5 kV at a flow rate of 2 mL/min. Form the experiments

conducted there seems to be a nonlinear response between the applied voltage and the transformation efficiency. Take into consideration the transformation efficiency at a flow rate of 1 mL/min. The maximum transformation efficiency of the sample at the specified flow rate of 1 mL/min is observed at 2 kV, and then the samples transformation efficiency decreases dramatically. Within the experimental domain chosen, there seems to be an optimal condition under which the electroporation parameters could be combined to optimize the system. Using the cuvette devices as a reference for the performance of the flow-through device, it can be seen that efficient transformation only occurs in the cuvettes at >2 kV. Throughout the experimental conditions shown, the transformation efficiency of the MFP tips were obtained at applied voltage that was half (1 kV) of those necessary to induce transformation in the *E. coli* DH10β. The hydrodynamically enhance MFP tips have shown greater efficacy than cuvettes when the MFP tips transformation efficiency are averaged by the flowrates. The experiment confirms that the MFP tip have outperformed the cuvettes devices. In addition the MFP have enable greater transformation efficiency at less applied potential difference, therefore enable the reduction and energy requirement for the electroporation process.

4.5: Waveform and Polarity Impact on Flow-Through Electroporation in Straight Channel Microfluidic Device at 2.5 kV

Table 3: The list of parameters introduced in the experiment in order to investigate the impact of polarity and waveform parameters' impact on the transformation efficiency of the *E. coli*.

Parameters	***Values***
Flowrate (mL/min)	1
OD_{600}	7.5 ($6x10^9$ cells/ml)
Conductivity of cells with DNA	73 µS/cm
Waveform List	(α-β): 0-160, 0-320, 0-640, 0-1280 µs at 2.5 kV (α-β): 10-160, 0-320, 0-640, 0-1280 µs at 2.5 kV
Control cuvettes parameters	1.25 kV, 1.75 kV and 2.5 kV ; τ= 1.5ms
Voltage applied (kV)	2.5
Devices	Polydimethylsiloxane (PDMS) Straight channel Chips vs Cuvette

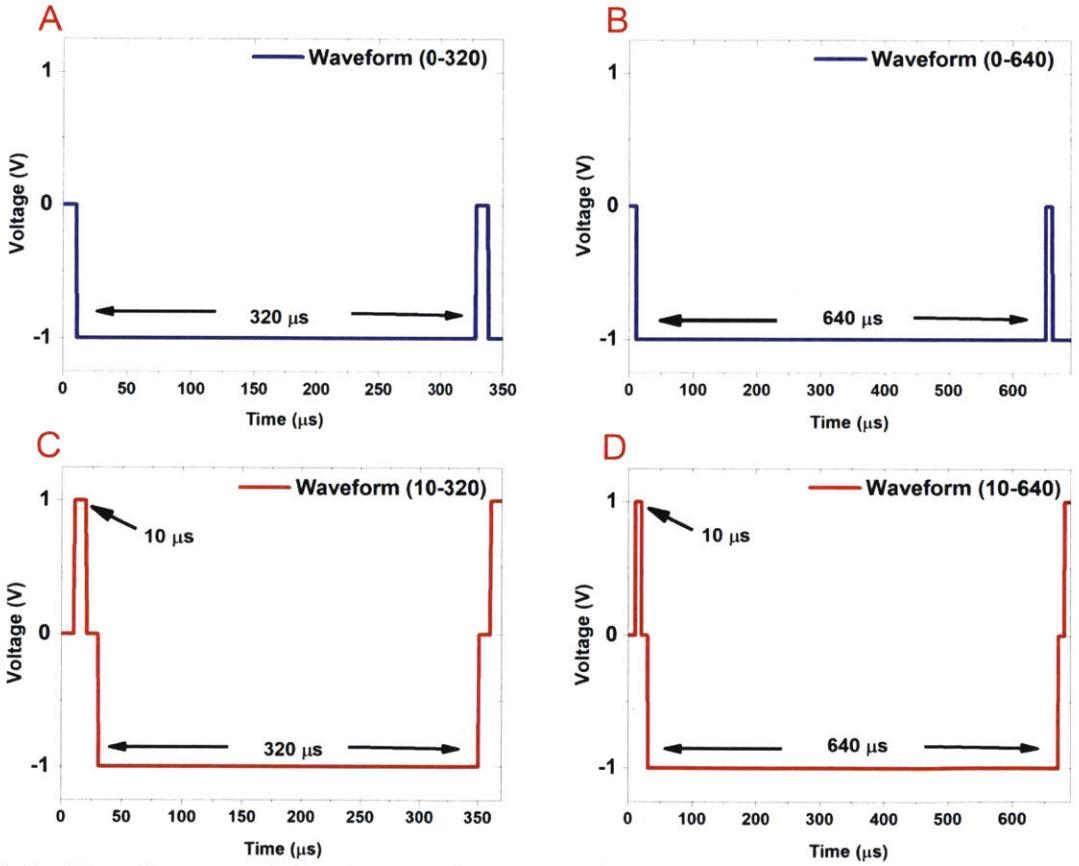

Figure 4-3: Waveforms used in the experiment to observe the effects of asymmetric pulses on electroporation efficiency. Plots are designated as A(10-160), B(10-320), C(0-160) and D(0-320). The waveforms labeled with 10, (10-160, 10-360…) observe a 10 µs alternative polarity during the electroporation process. The labels with 0, (0-160, 0-360…) observe a no pulse in the opposite polarity.

Asymmetric waveforms were developed during the electroporation process to investigate the effect of asymmetric pulses on the transformation efficiency of *E. coli*. The theory behind asymmetric waveform application is that the charged molecules would experience none zero displacement if the polarity shifts

were not equal. The asymmetric waveforms developed for electroporation was supplied with the use of a signal generator (Tabor Electronics WS8352 Arbitrary Waveform Generators). The signal was then amplified 1000X with a high voltage amplifier (Trek Model 623B High-Voltage Power Amplifier). The electrical connectors are then added to the device electrodes in order to supply the energy for the electroporation process. The designed signal will be coded with an index of (alpha-α, beta-β) to specify an individual waveform supplied to the cells. Here, alpha represents the time span in microsecond of the initial asymmetric peak and beta represent the secondary time span of the asymmetric peak in microseconds. The value of α is either 0 μs or 10 μs in its application during the experimental process. The range of values for β are 160 μs, 320 μs, 640 μs, and 1280 μs for the experiments undertaken.

Figure 4-3 shows some of the designed waveforms that were used in the experiments. Figure 4-3A is labeled as 10-160 and Figure 4-3B is labeled as 10-320 waveforms. These waveforms are bipolar in their delivery of the pulse, which switches between 1 and -1 volts before amplification. The pulses also have a 10 μs delay before switching between the polarities as can be seen in Figure 4-3A/B. The α=0 μs waveforms that are unipolar in design can be seen in Figure 4-3C and Figure 4-3D. Figure 4-3C shows the intended design of 0-160 waveform that switch to zero polarity (off) for 10μs before returning -1/+1 volts. Figure 4-3D, shows the 0-320 waveform, which similar to 10-160 but has a larger β time span and the same 10μs time span at zero volts. During the experiment, we collect the oscillography of the applied waveform in order to have reference of the output performance of the signal generator.

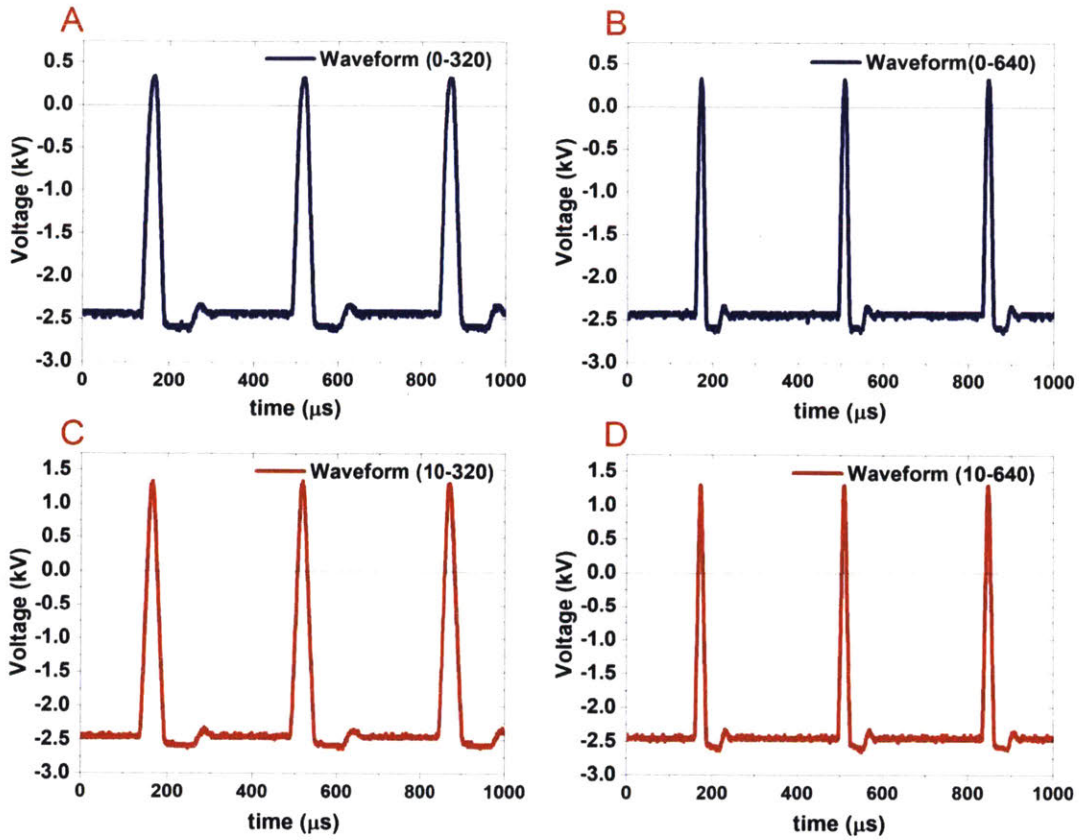

Figure 4-4: Output waveforms that are created by the function generator at the designed α-β values. The oscillography shows that the designed waveforms were distorted due to over/undershoot at various region. These variations of the output signal could in fact introduce uncontrollable effects on the transformation efficiency due to the introduction of distorted values of electric field strength or the time span of electric field exposure.

During the experiments, it has been observed that the designed waveform are distorted in the experiment due to overshoot/undershoot by the function generator. The actual output performance of the signal generator could have significant impact on the transformation efficiency of DH10β. For example, Figure 4-4A and Figure 4-4-B are α=0 μs waveforms, which show an observable overshoot at the designed zero potential. The concern is whether the overshoot has significant impact on the transformation efficiency because the peak-to-peak (P2P) amplitude are significantly different from the intended design. P2P is defined here as the maximum versus the minimum value of the waveforms. In Figure 4-4A the intended design was 2.5 kV P2P but the output of the signal generator was 2.99 kV P2P. Figure 4-4C and Figure 4-4D are the oscillography of α=10 μs waveforms. These designed waveforms are also distorted, and show some degree over/undershoot throughout the experiment due to the lack at reaching the peak value of 2.5

kV at α=10 μs. The calculated P2P values for Figure 4-4C and Figure 4-4D are 3.95 kV P2P and 3.97 kV P2P respectively versus their intended design, which is 5 kV P2P. The overshoot of the designed wave can have significant amplification of the electrified field distribution that the *E. coli* senses during the experiment. Therefore these parameters are noise factors that should be monitored throughout the experimental process in order to identify trends. Proceeding to experiment results we can see the effects of the waveforms and the polarity on the transformation efficiency at 2.5 kV.

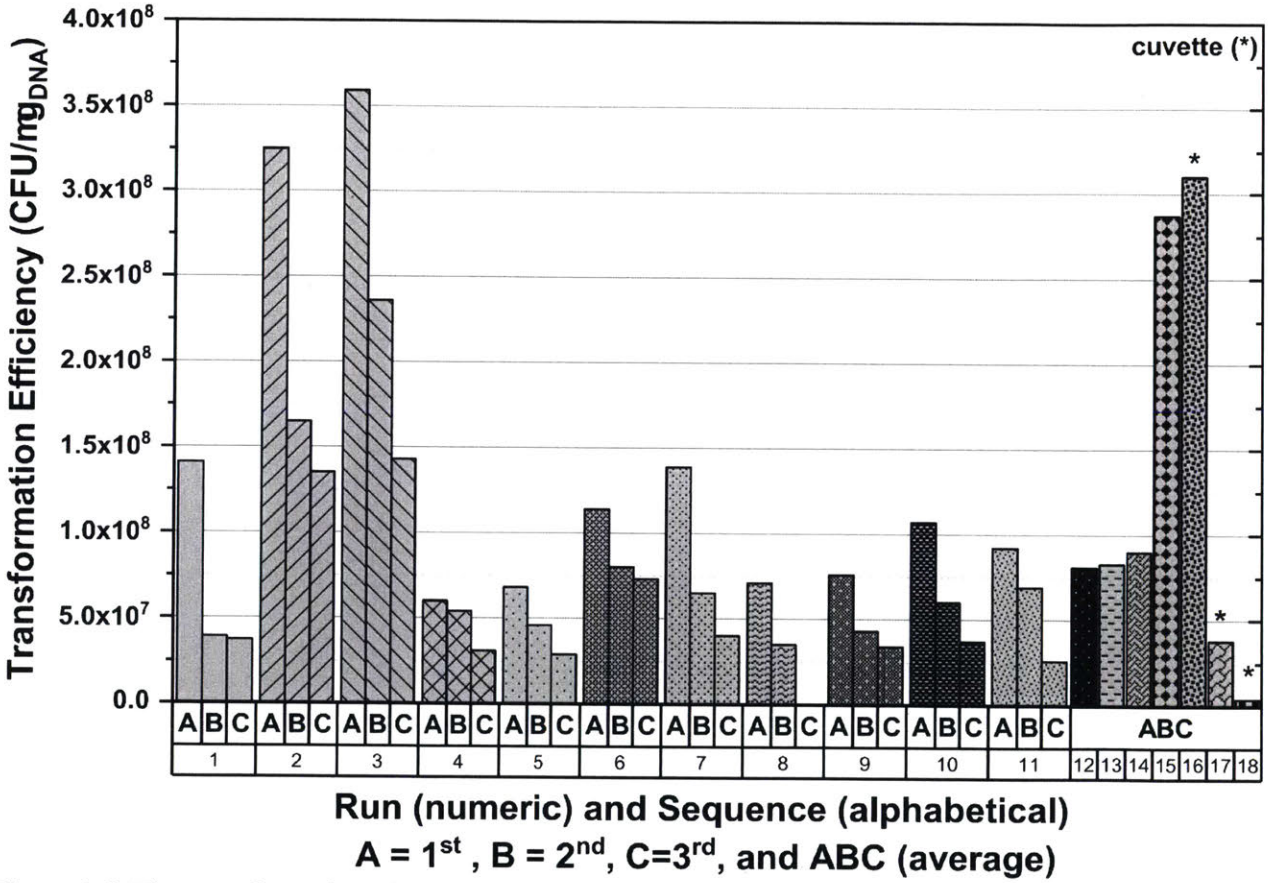

Figure 4-5: The transformation efficiency versus sequence and run in the experiment. Level 1 indicates the replicate (a=1st , b=2nd and c=3rd) and their transformation efficiency throughout the experiment. level 1 also contains an ABC index which are the averages of the experiments. Level 2 indicates a new parametric variation on the experiments, specfifically waveform, and they are labeled with numbers (1,2,3…18). As can be seen from the plot, the highest transformation efficiency was observed in exerpiment 3A which was completed at 0-640 waveform in the straight channel devices. The device also show a deterministic response to be repeated used throughout the experiments, where each squence during a run show a reduced transformation efficieny.

To investigate the transformation efficiency and its interaction with run and the sequence we have plotted Figure 4-5, the transformation efficiency versus run and sequence. In Figure 4-5 the transformation

efficiency versus the indexes of sequence at row one (level 1) and run at row two (level 2). The sequences of the experiment are labeled as A, B, C, and ABC (in particular situations where the replicates are averaged), are given as an index. The experimental run are listed on row two with notations that are numerical in value to indicate the unique parameters of the waveform that was applied during the experimental procedure. Upon further investigation, we see interesting correlation in the plot of Figure 4-5. One can observe the reduction in transformation efficiency per run as the replicate of the experiment progresses (A to B to C). The stared data point in Figure 4-5 shows the devices that are genetically transformed using the cuvette devices. Further investigation into the parameters waveform impact on the transformation efficiency leads to the plot in Figure 4-6.

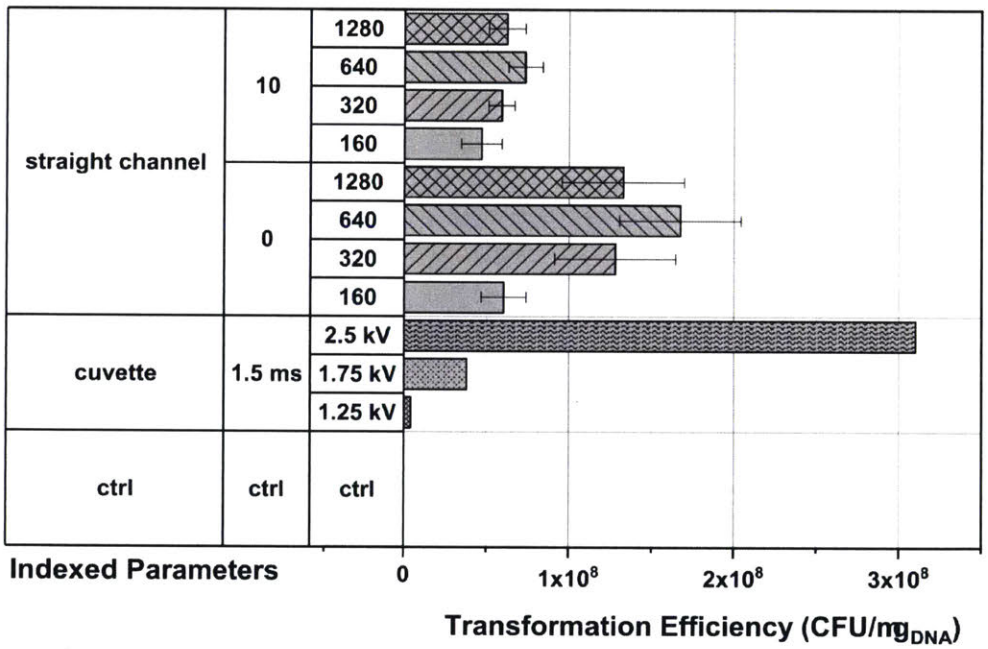

Figure 4-6: Bar plot of the transformation efficiency indexed to the waveform parameters α and β and the devices used during the specific experiment. For the cuvette devices, the decay waveform was used, therefore they are indexed in regards to voltages applied in the cuvette devices. The straight channel devices at β=640 μs is the highest performing average transformation efficiency for flow-through device. For the cuvette devices, it can be seen that as the applied voltages increases, so does the transformation efficiency. The control samples (ctrl) consistently produced zero transformations.

In Figure 4-6, the transformation efficiency of the devices is investigated with respect to the devices and waveform type used during the experimental run. The parameters are indexed into a table on the left-hand side of the bar graph. The corresponding row of the bar plot identifies the specific waveforms, the

average transformation efficiency, and the corresponding standard error of the mean error-bar (±1 sigma) (the standard error of mean is used for all plots with error bars). The waveform types of the straight channel devices are segmented into parameters α and β to define each uniquely. In the case of the curette devices tested during the experiment, Figure 4-6 is indexed in regards to the device (cuvettes), time constant, τ in milli-seconds (ms) and the applied voltage, since the waveform that is used by the Bio-Rad Micropulser™ electroporator is a decay function.

From Figure 4-6, focusing on experiments at α=10 μs, the highest transformation efficiency that was demonstrated during the experiment for the all the applied βs was 7.4×10^7 CFU/(μg_{DNA}). For experiments conducted with α=0 μs, the highest average transformation efficiency was 1.7×10^7 CFU/(μg_{DNA}) for all the applied βs. Interestingly, the highest performance at which both these prior stated transformation efficiencies occurred was at β=640 μs. From the bar plot in Figure 4-6, you can see that there exists at curved response to transformation efficiency as a function of β at each particular α timespan chosen. This brings forth the conclusion that the transformation efficiency can be optimized within the domain that we have investigated during the experiment. Focusing on the transformation efficiency observed for *E. coli* using the cuvette as standards. In Figure 4-6, it can be observed that the transformation efficiency increases as the applied voltages increases. For an applied voltage of 1.25 kV, 1.75 kV, and 2.5 kV the respective transformation efficiencies are 4.0×10^6 CFU/(μg_{DNA}), 3.8×10^7 CFU/(μg_{DNA}) and 3.1×10^8 CFU/(μg_{DNA}), respectively. The transformation efficiency of the control sample (ctrl) shows no colony forming units. Further investigation into the effects of the polarity of the electrodes on the transformation efficiency and the definition of polarity will be discussed in more detail.

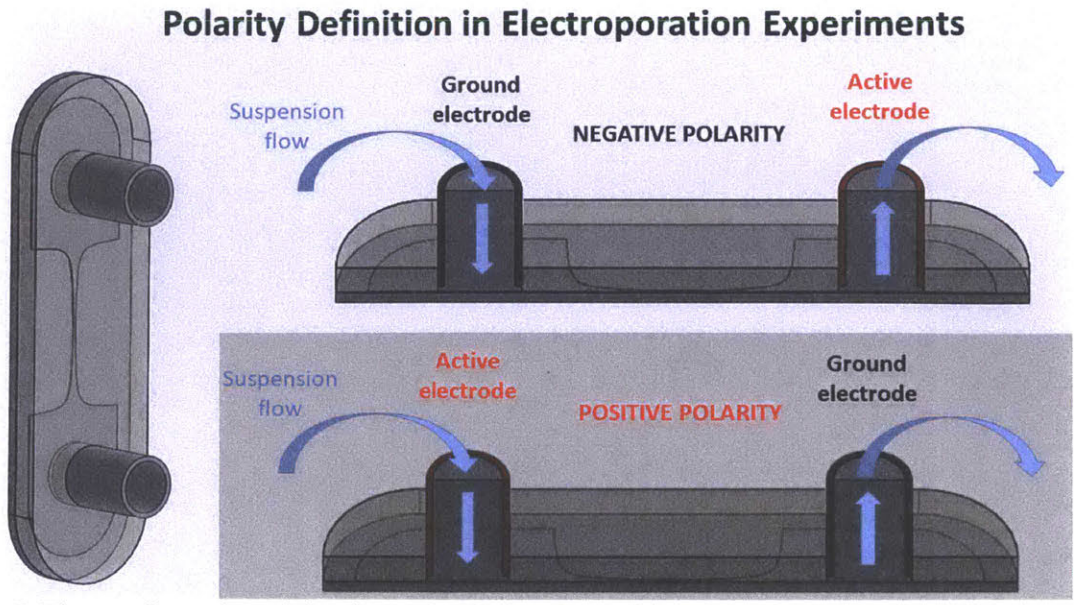

Figure 4-7: The configuration of the electrodes during the positive and negative polarity experiments using the geometrically constricted microfluidic chips. In the negative polarity experiments, the suspension of cells interact with the ground, electrodes of the microfluidic chips first then the suspension proceeds to interact with the active electrode as the suspension exits the device. The positive polarity is the opposite configuration of the negative. The active electrode's potential are exactly those seen by the α-β waveforms.

The configuration of the microfluidic chip (in this case the geometrically constricted channel) and the electrodes position during the experiment can be seen in the schematic developed in Figure 4-7. The negative polarity is defined as the left electrode being considered as the ground electrode. An alternative definition is that the ground electrode is the first to interact with the suspension of cells during the flow-through experiment on the microfluidic chips. The suspension then interacts with the active electrode as it exit the device. The positive polarity is considered the opposite of the negative polarity. Therefore, the definition of the positive polarity configuration, as can been seen in Figure 4-7, is the suspension of cells interact with the active electrode first during the flow-through experiments. The suspension then exits after passing through the ground electrode in the positive polarity configuration. We have used the term active electrode rather than anode or cathode because the waveforms that are used are not always unipolar (example, all α=10 μs time span waveforms). The active electrode represents the precise waveforms and potentials that are designed in Figure 4-4 from the oscilloscope. The effects of the variation of polarity and electrode configuration are also investigated during the flow through experiments on the straight channel microfluidic chips.

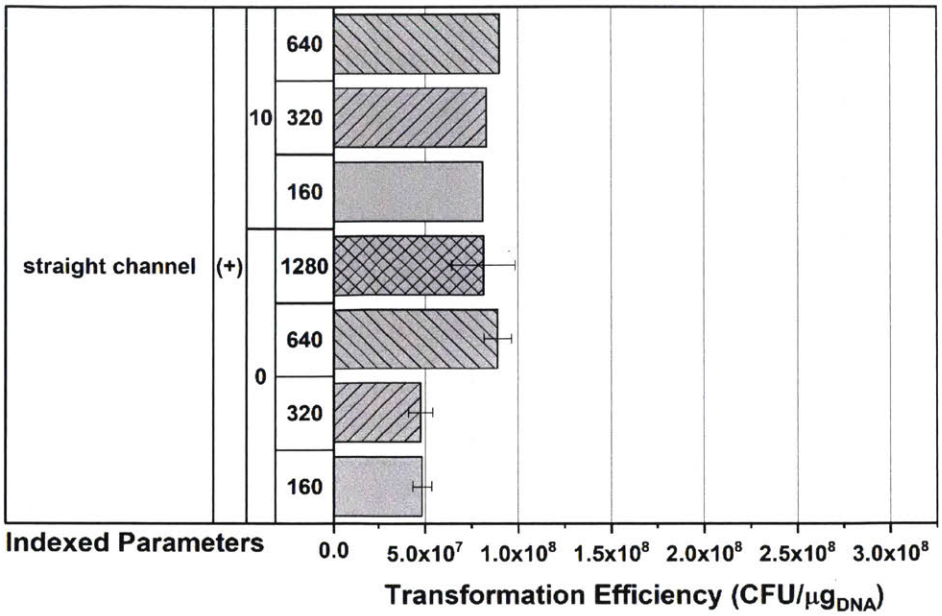

Figure 4-8: Effects of the positive polarity has on the transformation efficiency at the specific waveforms in the PDMS straight channel microfluidic chips. The waveforms that are α=0 μs show less transformation efficiency than α=10 μs when averaged over all β time spans conducted in the experiment. The maximum transformation efficiency seen using the positive polarity at α=0 μs and α=10 μs are observed at β=640 μs.

In Figure 4-8, the parameters are indexed in regards to the device, polarity of the electrodes, and then the α-β time spans with respective to the sequences. The maximum average transformation efficiency observed using the straight channel at positive polarity and α=0 μs was 8.9×10^7 CFU/(μg_{DNA}). This maximum transformation efficiency was also observed at a β time span of 640 μs, which support our previously stated results. The maximum efficiency of at α=10 μs and all applied β time spans was 9.0×10^7 CFU/(μg_{DNA}). Again the maximum averaged transformation efficiency for the experiment was for all particular α=10 μs experiments was completed at β=640 μs time span but the transformation efficiency of β=1280 μs was not completed during the experiment for the positive polarity study. The maximum transformation efficiencies at the positive polarity in comparison to the negative polarity are significantly different. Which indicates a significant impact from the electrode placement on the transformation efficiency.

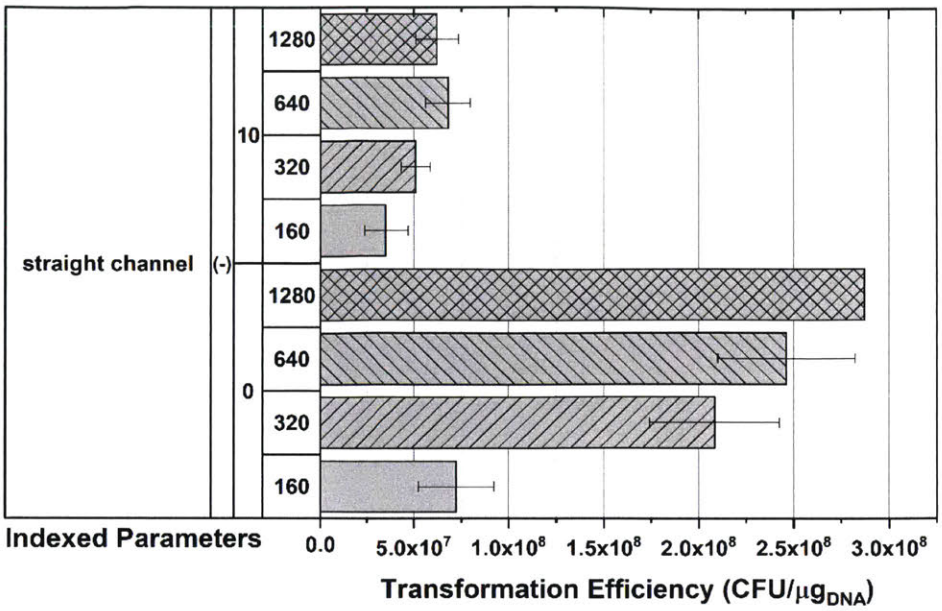

Figure 4-9: Effect of applying the negative polarity in the straight channel microfluidic devices for the electroporation experiments against the specific waveforms. The transformation efficiencies of α=0 μs parameters significantly outperforms α=10 μs experiments and those of the positive polarity. Interestingly, the correlation that was observed for β=640 μs seems to depart and the longer time spans for β increases the transformation efficiency at α=0 μs and negative polarity.

In Figure 4-9, the parameters are indexed in regards to the device, polarity of the electrodes, and then the α-β time spans with respective to the sequence. The maximum average transformation efficiency observed using the straight channel chips at negative polarity (-) and α=0 μs was 2.9×10^8 CFU/(μg_{DNA}). The data point was also average on the plates instead of by computationally averaging the CFU from three separate agar plates; therefore, no SEM error-bar was plotted on this data point. The deviation from the previously observed results could be due to the quantification method used. The maximum efficiency at α=10 μs and all applied β time spans was 6.8×10^7 CFU/(μg_{DNA}). Again we see that the maximum average transformation efficiency for the experiment for all α=10 μs experiments was completed at β=640 μs time span which correlates with previous observations. The overall effect of the negative (-) versus the positive (+) polarity for all the experiments has been dramatic.

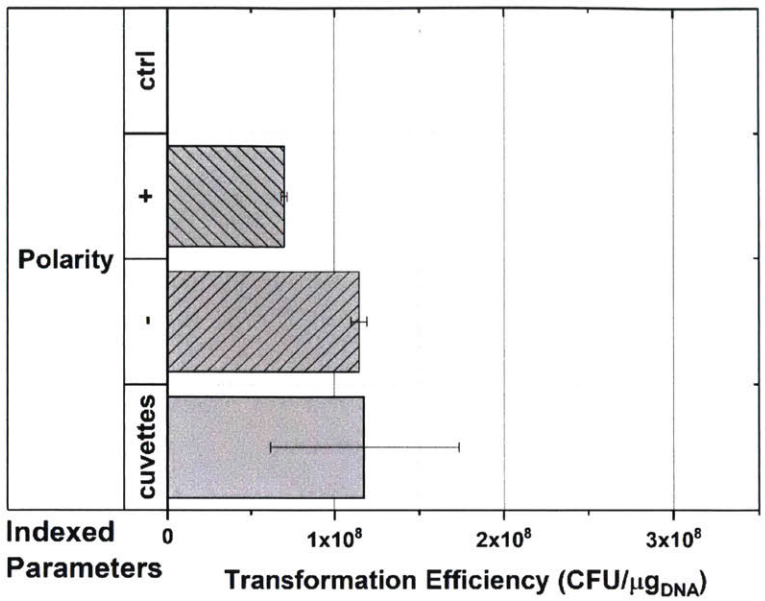

Figure 4-10: The transformation efficiency for all α-β time spans for the flow-through straight channel microfluidic chips versus polarity with referenced to the cuvettes performance. The positive polarity drastically reduces the transformation efficiency. We can see that the average transformation efficiency of the negative polarity is within the performance of the cuvette devices.

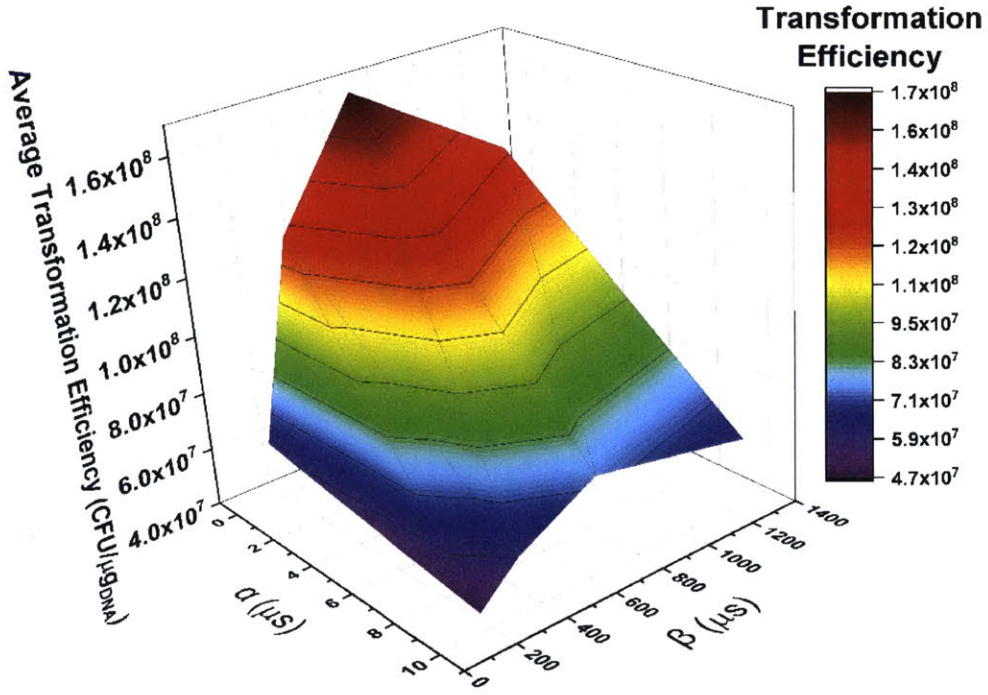

Figure 4-11: Projected response surface created for the α-β time span of the waveform and its effect on the transformation efficiency. Smaller α time spans increases the transformation efficiency of the electroporation process. In addition, the relationship between transformation efficiency and the β is nonlinear. B=640 μs was the most ideal for this experimental model.

In Figure 4-10, the parameters are indexed in regards to polarity that is used during the experiment for the straight channel microfluidic chips. The cuvettes and controls (ctrl) are plotted for comparative purposes. In Figure 4-10, the polarity dependent transformation efficiency plot shows that the positive (+) polarity of the electrode impedes the electroporation process. The negative (-) polarity is within the transformation performance of the cuvette devices. The comparing the performance between the negative (-) polarity and the cuvettes (consider as reference), we observe a 2% reduction in performance. Comparing the positive (-) polarity versus the cuvette, shows a 40% reduction in transformation efficiency.

Figure 4-11, shows the projected response surface for the averaged transformation efficiency versus α and β time spans parameters of the waveform. The surface shows that smaller value of α increase the mean transformation efficiency. The plot also shows optimal β parameters exist within the domain of the experimental conditions that we have chosen. At α=0 μs and β=640 μs, the mean transformation efficiency 1.7×10^{8} CFU/(μg_{DNA}) of the experiment condition exceeds all other parametric combination of α-β, regardless of the polarity used on the straight channel microfluidic chips.

4.6: Electroporation of E.coli with Waveform, Polarity, and Applied Voltage Variation

Table 4: The list of parameter introduced in the experiment in order to investigate the impact of polarity and waveform parameters in addition to voltages' effect on the transformation efficiency of the *E. coli.*

Parameters	***Values***
Flowrate (mL/min)	1
OD_{600}	10 ($8x10^9$ cells/ml)
Conductivity of cells with DNA	90 μS/cm
Waveform List (μs)	(α-β): 10-160, 0-320, 0-640, 0-1280
Control cuvettes parameters	1.25 and 2.5 kV; τ=1.5 ms
Voltage applied (kV)	1, 1.5, and 2
Devices	(PDMS) Straight channel Chips vs Cuvette

The experiment was conducted in order to investigate the effects of voltage on the transformation efficiency while using the asymmetric waveforms that were developed. We focused our efforts on the application of waveforms that are asymmetric, α=10 μs to observe the influence of the bipolar voltage peaks voltage's impact on transformation efficiency. The experiment was conducted in a similar manner to that of the previous experiment. The DH10β cells were made electro-competent and concentrated to an OD_{600} of 10. The electroporation was conducted in the straight channel microfluidic chips, the cuvettes were used as a reference to the chips' performance. The voltages applied to the suspension in the cuvette devices were 1.25 and 2.5 kV. The microfluidic chips were exposed to 1, 1.5, and 2 kV. The waveforms applied to the chips devices were α=10 μs and β=160 μs, 320 μs, 640 μs, 1280 μs. The specified flowrate for this experiment was 1000 ml/min as in the previous experiment. The specification of the experimental parameters can be obtained from Table 4. The performance of every experimental condition is plotted as a run chart.

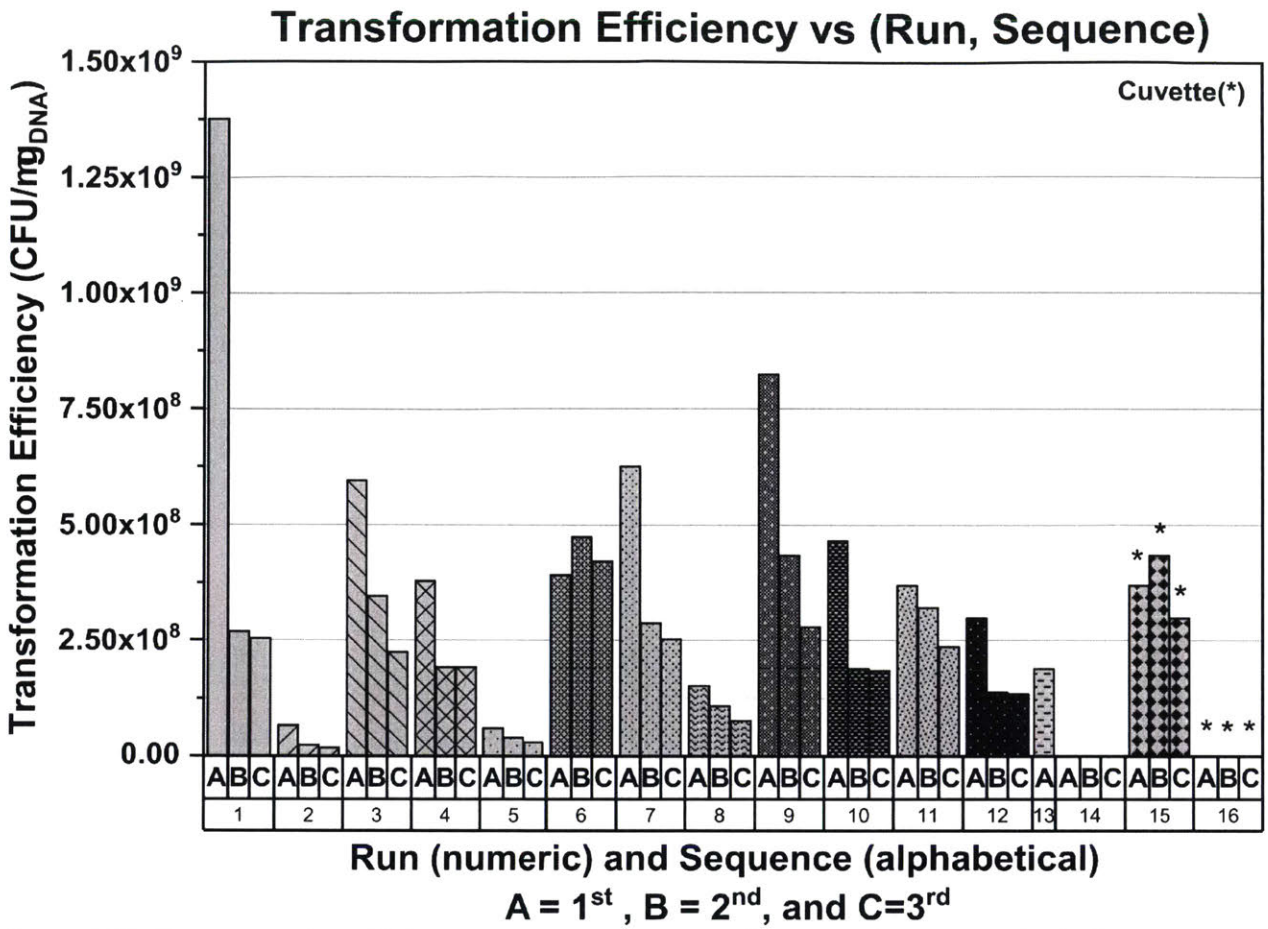

Figure 4-12: Transformation efficiency versus the sequence of the experiment. Level 1 indicates specific triplicate of the experiment (a=1st, b=2nd and c=3rd) on the experiment. Level 2 indicates a new parametric variation on the experiments and these are indicated with numerical values. As observed in the prior experiment, there exist a sequence reduction in the transformation efficiency as the sequence of the experiment progresses. The stared experiment are those conducted with the use of the cuvettes as a reference.

To investigate the transformation efficiency and the interaction with run and sequence we have plotted the run chart of the experiment, which can be observed in Figure 4-12. In Figure 4-12, the parameters are indexed in regards to sequence of the triplicates A, B, C and the experimental run. The experimental run are all independent variations of the applied voltages, waveforms, and polarity. As can be observed from the plot of the dataset, the sequential performance of the devices have a deterministic behavior as previously observed, where the transformation efficiency of A> B > C. The starred data points in Figure 4-12 are associated to the cuvettes' transformation efficiency. Sixteen experimental condition were tested. For experimental run 13, only one replicate was compiled since the data was average on the surface of the

agar plate. Experimental run 14 is negative control, which has shown zero colony forming units for each of the triplicates during the run. The highest transformation efficiency can be seen in experimental run 1, sequence A, at 1.4×10^9 CFU/(μg_{DNA}). The transformation efficiency of 1A will be treated as an outlier due to its significantly large value since it statistically impractical when in comparison to the means and the standard deviation of all the data within run 1. The assumption is that there was an error in the dilution or the plating protocol. Further investigation of the correlation between the parameters of the experiment leads to the plot in Figure 4-13.

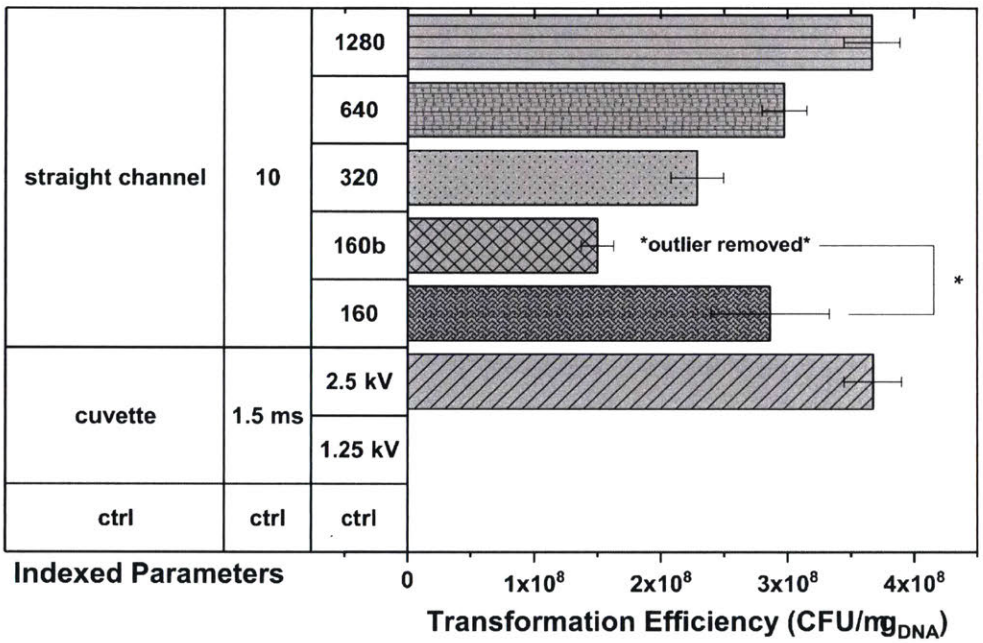

Figure 4-13: The transformation efficiency indexed to the waveform parameters α and β applied to the microfluidic chip. The cuvettes are indexed in regards to the two parameter associated to decay function, which are the time constant and the applied voltage as a reference. B=160b is the transformation efficiency with the outlier data point removed. As can be seen there exists a linear relationship in regards to the transformation efficiency and the β parameter. The control (ctrl) experiments show no transformation.

Figure 4-13 shows effects of the waveform on the transformation efficiency. The bar plot of the transformation efficiency indexed in regards to the waveform parameters and the device used during the experiment to deliver the pulse. Specifically, the microfluidic chips are indexed in regards to α and β parameters. The cuvettes are indexed in regards to the waveform parameter of the decay function, τ, and the applied voltage. During the experiment, no colony forming units were observed for cuvettes at an applied voltage of 1.25 kV and a time constant of 1.5 ms. The control samples show positive results due to

the lack of colony forming units. As can be observed from Figure 4-13, there exist a linear correlation between the β parameter and the transformation efficiency within the experimental parameters investigated in this study. This correlation is very interesting since in the prior experiment, the relationship was nonlinear and an optimum could be observed within the domain of β between 160 μs to 1280 μs. In addition, we can see that the maximum transformation efficiency is observed at α=10 μs and β=1280 μs at a value of 3.7×10^8 CFU/(μg_{DNA}) for the microfluidic chips. The maximum transformation efficiency for the cuvettes was observed at 2.5 kV at a value of 3.7×10^8 CFU/(μg_{DNA}) which is the same transformation efficiency as that of the microfluidic chip's maximum transformation efficiency. Investigating further, we see an interesting observation when considering the voltages applied to suspension of cell and the effect on the transformation efficiency.

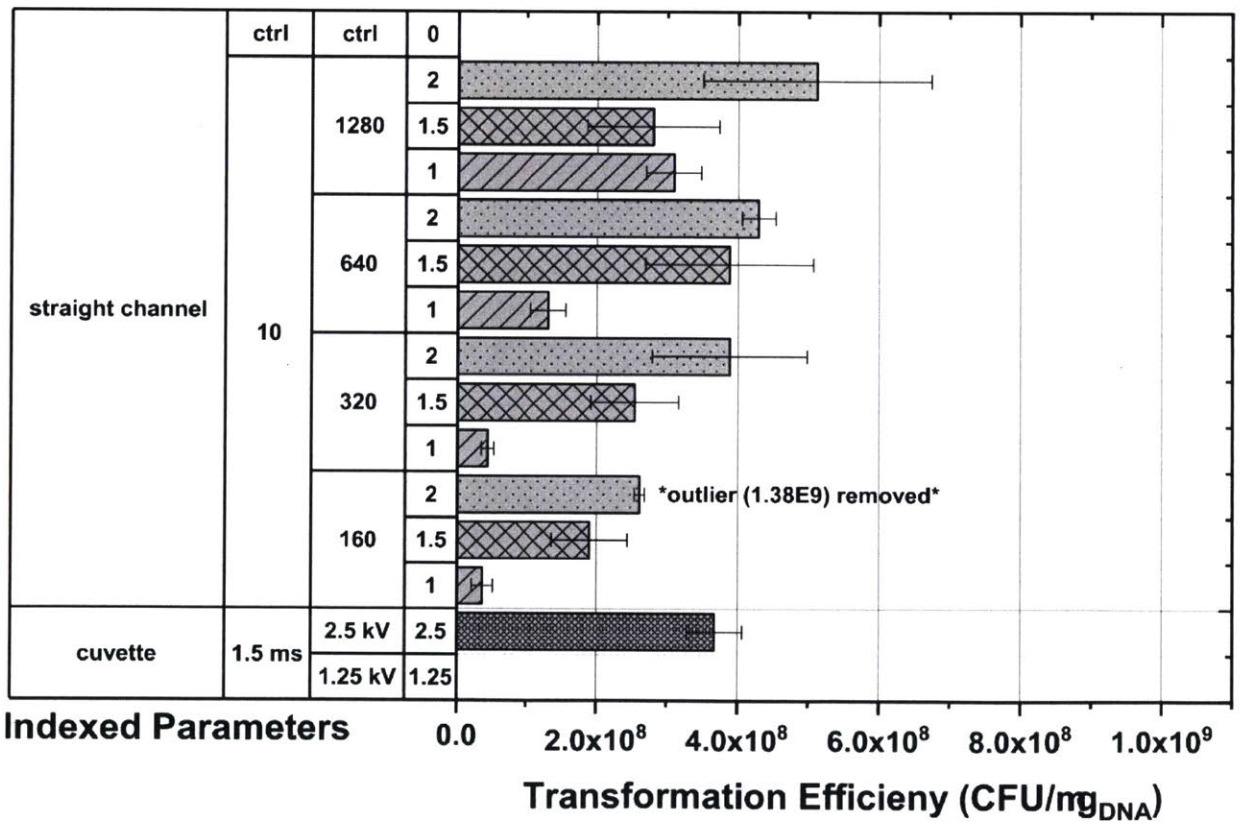

Figure 4-14: Transformation efficiency indexed by the applied voltage, waveform parameters, and the device used during the experiment. The results of the plot indicate that electroporation with higher transformation efficiencies can be obtain at less applied voltage with the use of the straight channel microfluidic chips.

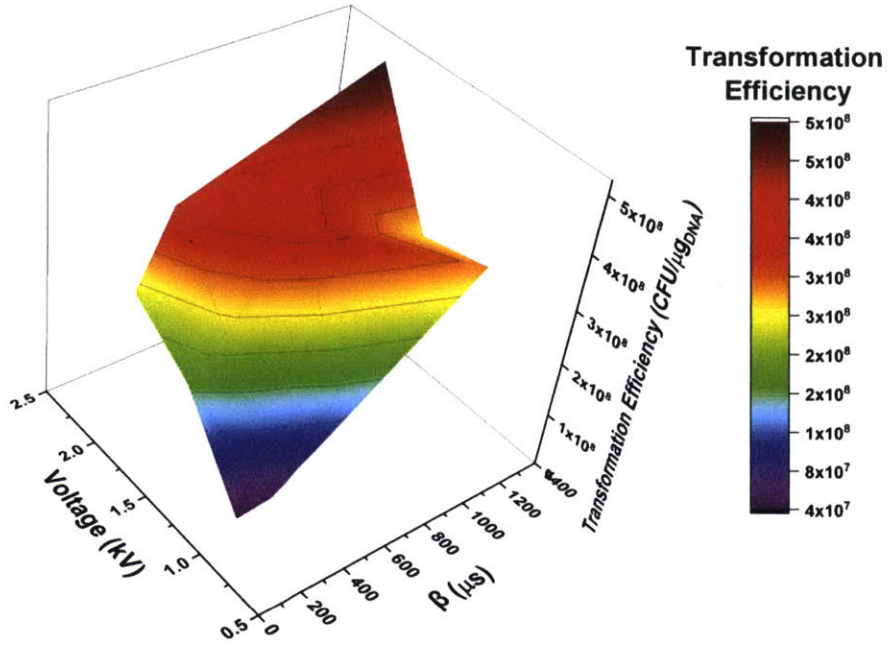

Figure 4-15: Transformation efficiency as a surface response. The transformation efficiency is a function of the applied voltage and the applied β time spans at α=10 μs. The figure shows that the transformation efficiency increases as the applied voltage and the β time span increases. The correlation departs at an applied voltage of 1.5 kV.

Here we investigate the impact of the variations of the applied voltage and the waveform and its correlation to the transformation efficiency. Figure 4-14 is indexed in regards to the devices, the wave parameters, α-β, and the applied voltages. In regards to the cuvette devices, they are again indexed to the decay functions parameters τ and the maximum applied voltage. The most important factor observed from Figure 4-14 is the fact that the maximum transformation efficiency is observed at α=10 μs, β=1280 μs and an applied voltage of 2 kV for with the use of the microfluidic chip when compared to all other experiments. The averaged transformation efficiency observed from the chip at α=10 μs, β=1280 μs and 2 kV was 5.1×10^8 CFU/(μg_{DNA}). This performance is 39% more efficient than that of the cuvettes' transformation efficiency at 2.5 kV. The cuvettes, operated at 2.5 kV, obtain a transformation efficiency of 3.7×10^8 CFU/(μg_{DNA}) during these experiments. Figure 4-15 show the transformation efficiency response surface as a function of applied voltage and the β time spans parameters of the waveform at constant α=10 μs. An observation from the experimental results is that as β increases so does the transformation efficiency when considering the application of 1 kV and 2 kV during the experiment as seen in Figure 4-15. This β parameter

correlation between transformation efficiency departs when considering the application of 1.5 kV and shows a similarity to the prior experiment conducted where there exist at optimal transformation efficiency at β=640 μs. The optimal electroporation condition can also be observed at the specified 1.5 kV can be observed in Figure 4-15. The study was completed at a single polarity since the prior experiments indicated that the positive polarity significantly reduces the transformation efficiency of the electroporation process.

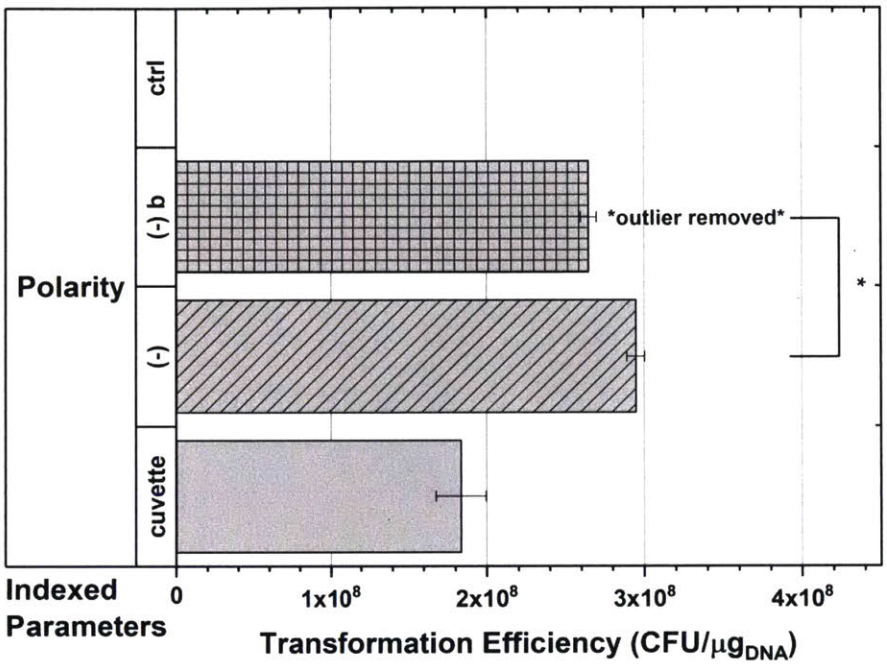

Figure 4-16: The transformation efficiency of negative polarity vs. the cuvette devices. As indicated by the plot, the average electroporation efficiency is greater in the microfluidic chips than that of the cuvettes. The applied voltage in the devices is coupled in the plots, so only the polarities are considered.

Figure 4-16 shows the indexed bar plot of transformation efficiency versus the polarity used during the experiment compared to the cuvette as a reference. Throughout the experiment, the average transformation efficiency of the microfluidic chip has outperformed that of the cuvette devices. The negative polarity (-), and the negative polarity with the outlier data point removed is listed as (-) b in Figure 4-16. Overall, the average transformation efficiency of microfluidic chip is 44% more efficient than the cuvettes. All experiments that were conducted with the microfluidic chips were completed at less voltage than the cuvettes.

Chapter 5

Unexpected Phenomena that Affected Electroporation

5.1: Introduction

Chapter 4 introduced the experimental parameters investigated throughout this thesis. Experimental data shows a 2.5 time increase in transformation efficiency for the MFP in comparison to the transformation efficiency of the cuvettes. The prior chapter also indicated that the polarity of the electrode placement used during the experiment plays a significant role in the transformation efficiency. This correlation is not yet fully understood. Therefore, in Chapter 5 we hypothesize some of the reasons behind this change in transformation efficiency. In addition, something that is of tremendous interest is the total energy absorbed by the fluid per unit volume during the electroporation experiment. Therefore, the liberty has been taken to project some of transformation efficiency of the MFP tips and cuvettes on to an energy related plot in order to identify any correlations.

5.2: Electrode Placement and its Effect on Transformation Efficiency

An interesting relationship that is obtained from analysis of the polarity dependence is the fact that there exist at 40% reduction in transformation efficiency due to choosing a positive polarity configuration

in the flow-through experiments. The electrical potential difference across the micro fluidic channel is altered in terms of its direction but the magnitude remains the same after the polarity is changed. A theory developed is that the DNA molecules have a different electrophoretic mobility than the *E. coli.* This difference in the electrophoretic mobility increases the interaction in specified directions due to the molecules attraction to a preferred electrode. This increases the rate of interaction between the DNA and cells during the electroporation process; if the preferred electrode configuration is used during the experiment. This is assuming that the dominant method of transformation during electroporation is due to electrophoresis. An alternative hypothesis that can be developed to account for possible chemical reactions at the electrode, or mass transport of the charged molecules towards their respective electrodes, assuming they have overcome advective transport forces. Further investigation will need to be completed in order to understand the fundamental principles behind the polarity dependence of transformation efficiencies. A more thorough and controlled experiment on this parameter will indeed give better insight into the mechanism by which exogenous material is transported through the cell membrane.

5.3: Cumulative Energy Delivered to Cells

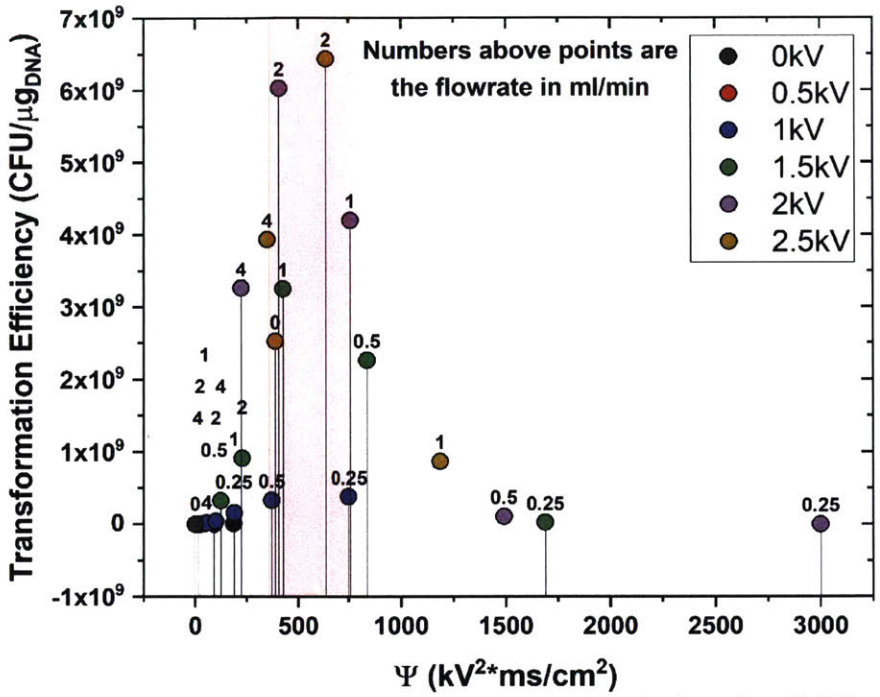

Figure 5-1: Squared electric field integrated over the residence time in the microfluidic pipette tips. The plot shows that the optimal operating region for the flow-through experiment is approximately 500kV^{2}ms/cm^2.

The dependence of the transformation efficiency on the magnitude of the electric field is well studied in terms of the required thresholds to induce electroporation. Therefore, a projection of the total electric field experienced by the bacteria might be a critical factor that determines the transformation efficiency. Since the microfluidic flow-through experiments are conducted while varying a specific controllable parameter such as the flowrate and applied voltage, the desire is to couple this information to the electric field. The underlining assumption that was developed is that the overall transformation efficiency is a multifaceted process but the most important parameter might be the total power per unit volume that the cells are exposed to during their residence time. From the correlation between the electric field and power, an alternative projection of the data was developed. The projection can be seen in Figure 5-1. The plot show the cumulative electric field squared versus transformation efficiency. We have defined a new parameter variable for the cumulative integral of electric field squared:

$$\Psi = \int E(t)^2 \, dt$$

The residence time is a function of the flowrate; therefore, as flowrate increases, Ψ is reduced. As the applied voltage increases, Ψ increases. Figure 5-1, shows the electroporation efficiency versus Ψ. As can be seen from the figure, the optimal region for electroporation is approximately Ψ=500 $kV^2 \cdot ms/cm^2$. The major factor of interest is that the flowrate the flow rate and applied voltage are coupled. Therefore, there seems to be no significant relationships between flowrate and transformation efficiency independently. The next interesting factor is that there seems to be a minimum required applied voltage to induce transformation. For instance, experiment conducted at Ψ=750 $kV^2 \cdot ms/cm^2$ shows that 1 kV applied voltage does not induce significant transformation efficiency but 2.0 kV applied at Ψ approximately equal to 500 $kV^2 \cdot ms/cm^2$ induces eight times the transformation efficiency at twice the applied voltage.

The electric field squared relationship is due to: $P/(\sigma Ax)=E^2$ from the relationship $J=E\sigma$ and $P=I^2R$. Where P is the power, σ is the conductivity, A is the cross section areas of the current flow, x is the length of the volume, E is the electric field, J is the current density, I is the current, $J=IA$ and R is the resistance. "$kV^2 \cdot ms/cm^2$ correlates to $(P/V\sigma)$ or power per unit volume times the material's resistivity.

Chapter 6

Conclusion

Electroporation has been limited to minute volumes of approximately 50μL throughout history. The transition to flow-through microfluidic device has increased the overall throughput performance of the process when compared to cuvette technology that is currently used in academia and industry. The additional hurdle that is tackled throughout this endeavor is the incorporation of the flow-through microfluidic electroporation technology to a high throughput liquid handling platform. Through design iterations, the development of a series of designs have been established that account for continuous flow conditions and manufacturability. The development of a microfluidic pipette tip, that has been translated from the microfluidic chip technology, has successful outperform the current state of the art at a variety of operating conditions. The maximum output transformation efficiency on *E. coli* DH10β for the MFP tip was 6.4×10^9 CFU/(μg_{DNA}). The output performance of the cuvette electroporation process was 2.5×10^9 CFU/(μg_{DNA}); which is less than half the performance of the MFP tips.

Investigating the asymmetric wave function during the experiment lead the discovery that $\alpha=0$ μs or unipolar waveforms applied to the electroporation process were optimal. The β parameters optimal condition during the experiment was 640 μs for electroporation, under the condition that were explored in the study. In addition, a major parameters that determines the electroporation process's efficiency is the electrode polarity. Through the study, it has been observed that when the flow front meets the ground electrode first (negative polarity), there exist a higher transformation efficiency. The application of a positive polarity during the electroporation process in the flow-through design could lead to a 40% reduction in transformation efficiency.

Bibliography

(1) Chemical- and Viral-Based Transfection Methods http://www.bio-rad.com/en-us/applications-technologies/chemical-viral-based-transfection-methods?ID=LUSOOP49.

(2) Sharei, A.; Zoldan, J.; Adamo, A.; Sim, W. Y.; Cho, N.; Jackson, E.; Mao, S.; Schneider, S.; Han, M.-J.; Lytton-Jean, A.; et al. A Vector-Free Microfluidic Platform for Intracellular Delivery. *Proc. Natl. Acad. Sci.* **2013**, *110* (6), 2082–2087.

(3) Transfection http://www.biontex.com/america/transfection.

(4) Electroporation http://www.bioelectrochemical-soc.org/general/electroporation.ph (accessed Jun 5, 2018).

(5) Wang, H.-Y.; Bhunia, A. K.; Lu, C. A Microfluidic Flow-through Device for High Throughput Electrical Lysis of Bacterial Cells Based on Continuous Dc Voltage. *Biosens. Bioelectron.* **2006**, *22* (5), 582–588.

(6) Huang, Y.; Rubinsky, B. Flow-through Micro-Electroporation Chip for High Efficiency Single-Cell Genetic Manipulation. *Sensors Actuators A Phys.* **2003**, *104* (3), 205–212.

(7) Yun, H.; Hur, S. C. Sequential Multi-Molecule Delivery Using Vortex-Assisted Electroporation. *Lab Chip* **2013**, *13* (14), 2764.

(8) Lu, H.; Schmidt, M. A.; Jensen, K. F. A Microfluidic Electroporation Device for Cell Lysis. *Lab Chip* **2005**, *5* (1), 23.

(9) Garcia, P. A.; Ge, Z.; Moran, J. L.; Buie, C. R. Microfluidic Screening of Electric Fields for Electroporation. *Sci. Rep.* **2016**, *6* (1), 21238.